Journal of Neural Transmission
https://doi.org/10.1007/s00702-026-03166-4

RESEARCH

Spontaneous whole retinal degeneration in aged Beclin1 heterozygous mice

Francesca Biagioni[1] · Maurizio Forte[1] · Flavio di Nonno[1] · Carla Letizia Busceti[1] · Roberto Pinelli[2] · Violet Vakunseh Bumah[3] · Michela Ferrucci[4] · Gloria Lazzeri[4] · Sebastiano Sciarretta[1,5] · Giacomo Frati[1,5] · Francesco Fornai[1,4]

Received: 9 April 2026 / Accepted: 22 April 2026

Abstract

Retinal degenerative diseases range from rare inherited forms to common multifactorial disorders such as age-related macular degeneration, which is the leading cause of blindness in developed countries. Recent evidence identifies impaired autophagy as a key pathogenetic mechanism. In the disease process alterations of the outer retina start from the retinal pigment epithelium (RPE), to progress downstream in the inner retina leading to widespread whole retinal degeneration. Recent studies indicate that among autophagy-related proteins Beclin1 plays a relevant effect in sustaining retinal integrity, since it is induced by light exposure and it is placed at the intersection between mitophagy, lipophagy, and glycophagy, which are involved during retinal degeneration. The present study was carried out by profiting of *BECN1* heterozygous aged mice (BECN+/−), where RT-PCR and western blotting analysis confirmed the loss of both the primary transcript (*BECN1*) and protein (Beclin1) in the whole retina. Multiple converging techniques indicate a marked degeneration of RPE and photoreceptor layer, where a dismantling of proteins forming tight junction was documented. Inner retinal degeneration was extended within outer and inner nuclear layer. In the inner retina the expression of the detrimental protein alpha synuclein was increased concomitantly with a defect of autophagy markers. The study indicates a seminal role of Beclin1 in maintaining retinal integrity and it defines the vulnerability of various retinal layers in the spreading of Beclin1-dependent retinal degeneration. The potential of increasing the expression of Beclin1 through photobiomodulation is discussed, since it supports retinal integrity when amber/red light-induced stimulation occurs.

Keywords Beclin1 · AMD · RPE65 · ZO1 · Retinal degenerative disorders · Photobiomodulation

✉ Francesco Fornai
francesco.fornai@unipi.it; francesco.fornai@neuromed.it

Francesca Biagioni
francesca.biagioni@neuromed.it

Maurizio Forte
maurizio.forte@neuromed.it

Flavio di Nonno
flavio.dinonno.92@gmail.com

Carla Letizia Busceti
carla.busceti@neuromed.it

Roberto Pinelli
roberto@seri-lugano.ch

Violet Vakunseh Bumah
Violet.Bumah@sfasu.edu

Michela Ferrucci
michela.ferrucci@unipi.it

Gloria Lazzeri
gloria.lazzeri@unipi.it

Sebastiano Sciarretta
sebastiano.sciarretta@uniroma1.it

Giacomo Frati
giacomo.frati@uniroma1.it

[1] IRCCS Neuromed, 86077 Pozzilli, IS, Italy

[2] SERI, Switzerland Eye Research Institute, Lugano, Switzerland

[3] Department of Chemistry and Biochemistry Bush Mathematical Sciences, Stephen F. Austin State University, Building Suite 108, 1936 North Street, Nacogdoches, TX 75965, USA

[4] Human Anatomy, Department of Translational Research and New Technologies in Medicine and Surgery, University of Pisa, 56126 Pisa, PI, Italy

[5] Department of Medical-Surgical Sciences and Biotechnologies, Sapienza University, Latina, Italy

Published online: 04 May 2026

Introduction

Retinal degenerative disorders represent a vast number of diseases (Christoforidis et al. 2011; Randolph 2024; Wert et al. 2014; Roh et al. 2018; Duncan et al. 2024). These range from rare inherited conditions to common metabolic disorders (such as diabetic retinopathy) up to multi-factorial age-related macular degeneration (AMD) (Ghasemi et al. 2026). The latter represents the most common cause of blindness in developed countries (Augustin and Kirchhof 2009; Libby and Gould 2010; Modenese and Gobba 2019) and an effective cure, which is based on an in depth knowledge of the biology of disease is needed. Retinal degenerative disorders often recruit altered autophagy as a seminal disease mechanism (Wang et al. 2019; Kaarniranta et al. 2023). In line with this, defective autophagy in the outer retina, and mostly within retinal pigment epithelium (RPE), is proposed as a pivot to start AMD and other retinal degenerations (Jiang et al. 2025).

In fact, the vulnerability of RPE is grounded on strong metabolic needs related to high oxygen consumption (Datta et al. 2023) and degradation of proteins, lipids, sugars and cell organelles such as mitochondria. These undergo intense turnover mediated by cell clearing pathways such as proteasome and autophagy (Lenzi et al. 2016; Limanaqi et al. 2019; Ryskalin et al. 2019; Nita and Grzybowski 2023; Lazzeri et al. 2025). These pathways are very effective within RPE, where they operate under the influence of the enzyme complex named mechanistic target of rapamycin (mTOR) (Lazzeri et al. 2025; Kim et al. 2025; Chowdhury et al. 2025; Fang et al. 2026; Zhang et al. 2026). In this way, mTOR drives RPE to play a critical role in supporting photoreceptor function by enabling nutrients exchange and managing cellular waste. This is partly due to autophagy activation, which is seminal in sustaining retinal integrity, while it is impaired in AMD and other retinal degenerations (Golestaneh et al. 2017; Kaarniranta et al. 2023; Pinelli et al. 2025). Several proteins sustain autophagy within the retina. Among these, direct evidence is provided showing that mice knockouts for pro-autophagy proteins develop a phenotype mimicking AMD and generalized retinal degeneration as well as central degenerative disorders (Battaglia et al. 2003; Lazzeri et al. 2007; Squitieri et al. 2010; Yao et al. 2015; Blasiak and Kaarniranta 2022; Gurubaran et al. 2024). Conversely, overexpression of proteins involved in autophagolysosome clearance counteract retinal degeneration (Pan and Valapala 2023). Such a topic is under intense investigation, as shown by some studies spanning from mouse models to human patients. For instance, a recent study indicates a positive correlation between chaperonin containing TCP1 subunit 2 (*CCT2*), a pro-autophagy-related gene, and AMD in human patients (Wang et al. 2025). Conversely, the overexpression of the autophagy disrupting gene *MLST8*, which over-activates mTOR alters RPE and produces a phenotype mimicking AMD (Bammidi et al. 2025; Chowdhury et al. 2025). In this model the rescue of autophagy through the mTOR inhibitor Torin 1 protects from AMD-like retinal degeneration (Bammidi et al. 2025).

Despite such recent evidence, the specific involvement of classic autophagy initiating proteins remains non-investigated. This appears to be critical concerning fundamental proteins needed to initiate the autophagy progression such as Beclin1, which among several primary autophagy proteins is mostly involved in the removal of lipid droplets, glycogen granules and altered mitochondria (Li et al. 2014; Di Rienzo et al. 2024; Lazzeri et al. 2025; Pinelli et al. 2025), which are crucial in producing cell pathology during retinal degeneration (Shatz et al. 2024; Zhou et al. 2024; Jiang et al. 2025; Mohtashami et al. 2025; Li et al. 2025). In detail, Beclin1 was recently proposed as a kernel in regulating the crosstalk between mitophagy (Zhang et al. 2023), lipophagy (Singh and Cuervo 2012; Jarocki et al. 2024), and glycophagy (Koutsifeli et al. 2022; Mancini et al. 2023) which are mostly impaired during AMD (Pinelli et al. 2025). This is remarkable considering that Beclin1 sustains autophagy induced by microgravity (Liu et al. 2025a, b) and supports retinal integrity when light-induced stimulation occurs (Chen et al. 2013).

Therefore, the present study profits from a mouse model expressing a single allele of the gene coding for the autophagy protein (*BECN1* heterozygous mice; BECN+/-) to investigate the potential alterations within various retinal layers, which may develop in aged mice. The study was carried out at first, by using plain histochemistry with hematoxylin & eosin (H&E), 4′,6-diamidino-2-phenylindole (DAPI) and red oil to detect cell pathology and it is further grounded on immunostaining of specific antigens bound to RPE and outer retina, such as RPE-specific 65 kDa protein (RPE65), zonula occludens-1 (ZO1), and occludin or being associated with the autophagy pathway such as microtubule-associated proteins 1 A/1B light chain 3 (LC3) and lysosomal-associated membrane protein 1 (LAMP1). In addition, the detrimental protein alpha synuclein (alpha-syn) was stained within various retinal layers and the heterozygous condition for Beclin1 was validated by carrying out RT-PCR and western blotting from the whole eyeball.

Materials and methods

Animals and experimental design

A total of $N=22$ mice ($N=11$ BECN+/-, and $N=11$ wild type littermates, WT) were used in the present

experiments. Mice were purchased from Jackson Laboratory (B6.129 × 1-Becn1^{tm1Blev}/J, Cat# 018429, RRID: IMSR_JAX:018429) and they were bred at the animal facility developed and authorized at Istituto di Ricovero e Cura a Carattere Scientifico, IRCCS, Istituto Neurologico Mediterraneo, Neuromed (company code 038 IS 069) the experimental protocol was extended and approved by the Italian Ministry of Health for this specific study, authorization N. 804/2021-PR (code 30234.69).

Male mice were housed under controlled environmental conditions (temperature 22 ± 2 °C and relative humidity 50–60%) with a 12 h light/dark cycle and food and water *ad libitum*. In complaining with approved ad-hoc experimental protocols, all efforts were made to minimize animal suffering and to reduce the number of animals in keeping with statistical requirements, according to the European Guidelines, 2010/63/UE.

Since experiments were aimed at assessing age-related macular and inner retinal degeneration, mice were sacrificed at one-year age. The grouping of samples from BECN+/- and WT mice is reported in Supplementary Information.

One-year-old BECN+/- and WT mice were sacrificed under deep isoflurane (5%) anesthesia. From each mouse, both eyeballs were enucleated (total of 44 eyeballs from all mice). A total of 22 eyeballs per each group (11 × 2) were enucleated and processed as reported in the scheme uploaded within Supplementary Information. Briefly, according to the scheme: 4 right eyeballs from 4 different mice per group were collected to carry out RT-PCR for *BECN1* primary transcript and western blotting for Beclin1 protein (from the same eye). Eighteen eyeballs from each group (including the 4 contralateral, left, eyeballs from the 4 mice used for RT-PCR and western blotting and both eyeballs from 7 mice per group) were immersed in paraformaldehyde to be fixed. Seven fixed left eyeballs from seven different mice from each group (including the 4 contralateral, left, eyeballs from those mice whose right eyeball was used for RT-PCR and western blotting) were used in the present study to carry out histochemistry and immunohistochemistry aimed at detecting retinal integrity and the staining of specific proteins within retinal neurons. Eleven fixed eyeballs per group were stored for additional studies. From each group $N = 7$ fixed eyeballs were used both for histochemistry and immunohistochemistry. Immunostaining for Beclin1 was used to document differences concerning in situ protein expression between experimental groups to validate data obtained from RT-PCR and western blotting from the contralateral eyes of the same mouse. Histochemistry was carried out to assess neuronal integrity and counting neuronal loss. In detail, plain H&E histochemistry, and DAPI histofluorescence were used to assess whole cell and nuclear integrity, respectively, within various retinal layers. In addition, red oil was used to stain lipids. Immunostaining for those proteins which are crucial for RPE integrity was carried out by using antibodies staining RPE-65, ZO1, and occludin, which are key in the activity of RPE including formation of tight junctions (Bruban et al. 2009; Napoli et al. 2021; Napoli and Strettoi 2023; Ma et al. 2023). In fact, the loss of tight junctions is typical of AMD (Ma et al. 2023; Lazzeri et al. 2025). Antibodies against RPE65 mark a protein, which is key protein for shuttling the photoreceptors outer segment (POS) to RPE (Zhang et al. 2018), thus allowing degradation and recycling of POS (Tanabu et al. 2019; Postnikova et al. 2025). The outcome of the heterozygous condition for the allele *BECN1* in the expression of autophagolysosome-related antigens LC3 (autophagosomes) and LAMP1 (lysosomes) was assessed through LC3 and LAMP1 immunostaining. The occurrence of a classic protein related to neuronal degenerations such as alpha-syn was detected by immunofluorescence.

Tissue preparation

Real-time PCR for BECN1 in the whole eyeball

Total RNA from the retina of 4 WT and 4 BECN+/- male mice was extracted using TRIZOL (Thermo Fisher Scientific, Waltham, MA, U.S.A., Cat# 15596026) and it was quantified with a spectrophotometer. cDNAs were synthesized from 300 ng RNA using the SuperScript VILO Master Mix (Thermo Fisher Scientific, Cat# 11756050) and *BECN1* expression was calculated by reverse transcriptase quantitative RT-PCR using the ViiA 7 Real-Time PCR System (Applied Biosystem, Foster City, CA, U.S.A.) and SYBR Select Master Mix (Applied Biosystem, Cat# 4472908). All primers here used were designed according to sequences published on GenBank. The amount of target DNA was calculated by the comparative 2-DDCt method using glyceraldehyde 3-phosphate dehydrogenase (*GAPDH*) as a housekeeping gene. The following primers were used: *BECN1* sense: 5'-CAG CCT CTG AAA CTG GAC ACG A-3', antisense: 5'-CTC TCC TGA GTT AGC CTC TTC C-3'; *GAPDH* sense: 5'-CGT CCC GTA GAC AAA ATG GT-3', antisense: 5'-TCA ATG AAG GGG TCG TTG AT-3'.

Beclin1 western blotting of the whole eyeball

For immunoblotting, proteins from total eyeball ($N = 4$ WT and $N = 4$ BECN+/- mice) were extracted in RIPA lysis buffer system (Santa Cruz Biotechnology, Dallas, TX, U.S.A.), separated by SDS-PAGE and transferred into polyvinylidene difluoride membranes. Membranes were blocked with 5% non-fat dried milk (Bio-Rad, Hercules, CA, U.S.A.) and they were incubated overnight with primary polyclonal antibody

(rabbit anti-Beclin1, Cell Signaling Technology, Leiden, The Netherlands, Cat# 3738, RRID: AB_490837; 1:1000), and monoclonal antibody (mouse anti-vinculin, Santa Cruz Biotechnology, Cat# sc-73264, RRID: AB_1131292; 1:1000). Secondary antibody consisted of either horseradish peroxidase (HRP)-conjugated anti-mouse (Immunological Sciences, Roma, Italy, Cat# IS20400, 1:5000) in the case of vinculin or HRP-conjugated anti-rabbit (Immunological Sciences; Cat# IS20402) in the case of Beclin1. Immunoreactivity was assessed through ECL prime (Amersham Biosciences, Piscataway, NJ, U.S.A., Cat# RPN2236), where the chemiluminescent signal was detected by using a ChemiDoc XRS+with ImageLab software, and densitometry analysis was performed with ImageJ software version 1.2.4 (RRID: SCR_003070) (all Bio-Rad).

Morphology

From each group 7 eyeballs were fixed in 4% paraformaldehyde phosphate buffered solution (PBS) (Sigma Aldrich, Milan, Italy) (PFA), for 5 h, at 4 °C, to be further embedded in paraffin. Ten-µm-thick serial sagittal slices, at 100 µm intervals, were obtained along the medio-lateral extent of the retina (from nasal to temporal areas) for a total of 24 levels (2.4 mm). Counts were carried out in the three most central retinal slices in the effort to detect a region which covers the center of the visual field (the mouse retina does not contain a typical foveal area, Sze et al. 2025).

Retinal histochemistry

H&E

De-waxed slices from $N=7$ WT and $N=7$ BECN+/- mice were hydrated by serial decreasing alcohol solution (100%, 96%, and 70%) and further immersed in Mayer hematoxylin solution (Diapath, BG, Italy, Cat# C0302), for 8 min followed by eosin solution (Diapath, Cat# C0352), for 30 s. Stained slices were observed under a Zeiss (AxioImager M1, Zeiss, Oberkochen, Germany) microscope equipped with a Nikon DS-Ri1 camera (Nikon, Tokyo, Japan) connected to the NIS Elements software (Nikon, Tokyo, Japan) for image analysis.

DAPI

The marker DAPI (Sigma Aldrich, Milan, Italy; Cat# D9542, 1:300 for 3 min) was used to stain deoxyribonucleic acid, DNA, which is inferred as nuclear staining. In this way, nuclei could be selectively counted by using a Zeiss (AxioImager M1, Zeiss, Oberkochen, Germany) microscope under a filter allowing to detect blue fluorescence. The microscope was equipped with a Nikon DS-Ri1 camera (Nikon, Tokyo, Japan) connected to the NIS Elements software (Nikon, Tokyo, Japan) for the count of nuclei.

Red oil staining

De-waxed slices were stained with Oil-Red O Kit (Bio-Optica, Milan, Italy; Cat# 04-220923). The kit is composed of two different components: Oil-Red O, which selectively stains lipids in combination with hematoxylin, for nuclear staining. Slices were immersed in Oil-Red O for 20 min and quickly washed with tap water. The slices were further exposed to hematoxylin for 30 s and then washed for 3 min in tap water to be finally mounted in 80% glycerol. In this way, lipids appear as reddish material in the pale cytosol, where nuclei are stained in blue (hematoxylin).

All these histochemical procedures allow to count cell number, cell nuclei, linear extent and thickness of specific retinal layers. In this way, continuity, thickness and cell/nuclear density were counted within RPE, photoreceptor layer (PRL), outer and inner nuclear layers (ONL and INL, respectively) outer and inner plexiform layer (OPL and IPL, respectively) ganglionic cell layer (GCL) from each experimental group. Counts were carried out mostly by using 20X magnification through Image J software. Data were expressed as the mean ± SEM of areas or linear surfaces randomly chosen from three retinal slices, sampled at 100 µm interval, per each eye, from seven mice, from each experimental group.

Retinal immunohistochemistry

De-waxed slices were heated from 95 °C to 99 °C in citrate buffer (pH 6.0) for 20 min for antigen retrieval. Non-specific antigens were prevented from interacting with primary antibodies by a previous exposure to iso-specific normal serum for 1 h. Thereafter they were incubated overnight at 4 °C with various primary antibodies: (i) mouse monoclonal antibody anti-RPE65 (Novus Biologicals, Centennial, CO, U.S.A. Cat# NB100-355, RRID: AB_10002148; 1:100); (ii) goat polyclonal antibodies anti-ZO1 (Abcam, Cambridge, UK, Cat# ab190085, RRID: AB_2890613; 1:100); (iii) rabbit monoclonal antibody anti-occludin (Abcam, Cambridge, UK, Cat# ab216327, RRID: AB_2737295; 1:100); (iv) mouse monoclonal antibody anti-LC3 (Santa Cruz Biotechnology, Dallas, TX, U.S.A. Cat# sc-271625, RRID: AB_10714949; 1:100); (v) mouse monoclonal antibody anti-LAMP1 (Atlas Antibodies, Stockholm, Sweden, Cat# AMAb91170, RRID: AB_2665831; 1:100) (vi) rabbit polyclonal antibodies anti-alpha-syn (Sigma-Aldrich, Cat# SAB4502828, RRID: AB_10746104; 1:100). Technical control was performed without primary antibody. After

primary incubation, tissue slices were incubated for 1 h at room temperature with secondary fluorescein-conjugated anti-mouse antibody (Vector Laboratories, Newark, CA, U.S.A. Cat# FI-2000, RRID: AB_2336176; 1:100), or fluorescein-conjugated anti-rabbit antibody (Vector Laboratories, Cat# FI-1000, RRID: AB_2336197; 1:100) or fluorescein-conjugated anti-goat antibody (Vector Laboratories, Cat# DI-1488, RRID: AB_2336402; 1:100) or Cy3-conjugated anti rabbit antibody (Merk Millipore, Billerica, MA, U.S.A., Cat# AP182C, RRID: AB_92588; 1:400). After washing, slides were mounted with vectashield antifade mounting medium for fluorescence (Vector Lab., Cat# H-1000-10, RRID: AB_2336789) acquired by Axiophot2, Carl Zeiss Oberkochen (Germany) microscope.

Additional de-waxed slices were stained for Beclin1 expression by using immunoperoxidase as staining protocol. In detail, endogenous peroxidase activity was removed from the natural slices by previous incubation with 3% hydrogen peroxide (H_2O_2, 10 min at room temperature). Then, slices were plunged for 1 h, at room temperature, in a 10% normal horse serum solution to prevent non-specific binding of primary antibody. Slices were then incubated overnight at 4°C with the primary rabbit anti-Beclin1 antibody (Sigma Aldrich, Cat# B6186, RRID: AB_1078275; 1:100). As usual, negative controls were incubated without primary antibody. Slices were then incubated with a biotin-conjugated secondary anti-rabbit antibody (Vector Lab., Cat# BA-1100, RRID: AB_2336201; 1:100), for 1 h, at room temperature followed by streptavidin peroxidase (Vector Lab., Cat# SA-5004, 1:100), for 1 h, at room temperature. Slices were finally exposed to the peroxidase substrate 3,3'-diaminobenzidine (DAB, Sigma Aldrich, Cat# D4293) for a few minutes at room temperature. Finally, slices were dehydrated with increasing alcohol solutions (70%, 96%, and 100%), clarified in xylene and finally covered with mounting medium (Diapath, BG, Italy, Cat# 060200). Stained slices were analyzed at light microscopy Zeiss (AxioImager M1, Zeiss, Oberkochen, Germany).

H&E-stained slices allowed measuring the thickness of ganglion cell layer (GCL) and RPL and to count cell number within ONL and INL. This was carried out following a specific procedure, which was described below ("Extended statistics").

Count of nuclei in each retinal layer was carried out with the nuclear marker DAPI, as described below in "Extended statistics". Images at 20X magnification were used for quantification of the number of blue, fluorescent nuclei.

Extended statistics

This paragraph provides a description of statistical criteria adopted for data collection and inference analysis between groups. An additional part concerns the methods used to validate findings by combining various procedures.

Measurement of retinal layers (length, thickness, cell density)

H&E- and DAPI-stained slices were used for assessment of retinal integrity including staining intensity, neuronal shape, neuronal density, and cell ruptures. These histochemical procedures were used to count thickness, length and cell density within various retinal layers including length and thickness of RPE since continuity of this cell layer represents a critical issue which is lost in AMD. At this aim, DAPI staining was more effective than H&E since the optical interference produced by melanin impairs detection of single RPE cells through light microscopy. This was largely circumvented by histofluorescence, which affects minimally the melanin content. H&E staining instead was better employed to establish cell integrity in other retinal layers since both cytosol and nucleus were potentially visualized. Even thickness of various retinal layers but RPE was better established by H&E since the borders of each layer could be easily established. When assessing cell density or nuclear density, counts were carried out by using both H&E and DAPI, respectively, to define reliably the number of cells and nuclei within a given retinal area through a clear-cut definition of nuclear and cell size and shape. This was achieved by filtering primary authentic images through a conversion in 8-bit black and white images, which were than inverted by ImageJ software. In this way the fading of cell contour, which is naturally produced by analogic histochemical/histofluorescence staining was converted into a digital all-or-none signal, which produces a well-defined cell contour thus improving cell identification and cell count. The staining threshold was empirically established in preliminary samples and further applied automatically. The filtering of overlapping/fading staining was needed to provide clean numerical values useful for descriptive statistic, thus circumventing potential bias due to intense packaging of neurons, mostly occurring within INL and ONL. Consistently, the converted and inverted images appear polished from misleading background staining and polychromatism leaving in place only intense and well-defined H&E staining converted into black and white. In this specimen, contrast enhancement provided intensely stained structures, which were evident as defined white objects, while background staining was suppressed down towards the black tones. In the case of H&E the procedures provide an improved detection of cell contour while in the case of DAPI each specific nucleus was clearly marked avoiding artefacts due to densely packed overlapping nuclei within the specific cell layer. The count of cell/nuclear density was carried out

applying this method to standard retinal area (200 μm^2) being analyzed at 20X magnification. In each slice an average of 4 randomly sampled areas were counted. This was applied within each retinal layer under analysis. Since 3 slices were considered for each retina, a total of 12 areas per each layer were sampled from each retina. Considering that, in each group $N=7$ retinas were sampled, a total of 84 retinal areas from each group of mice was considered for each retinal layer. Thus, collected data from 84 areas per group allow to cast descriptive statistics which was expressed as the mean ± SEM. Inferential statistics between groups was obtained by comparing cell density in each retinal layer by applying Student's *t*-test (GraphPad Prism Software version 8.0.1, RRID: SCR_002798). Considering that inherent variability in the cell count produced by *BECN1* heterozygosity may affect randomly various retinal layers, the Student's *t*-test may have not covered the essence of the biological distribution of variance. Therefore, One-Way ANOVA was used in addition.

Details about conversion of primary images

Count of cells/nuclei within ONL and INL was carried out in H&E-/DAPI-stained slices. The same sampling used for the measurement of layer thickness (3 slices sampled at 100 µm interval for each retina, $N=7$ per group) was used for counting cells and nuclei. As reported, a major bias to count cell density in these retinal layers is due to non-defined cell borders generated by background of H&E staining produced by high cell and nuclear density. This fact may strongly affect clear identification of cell and nuclear contours. Therefore, cells and nuclei were counted using inverted 8-bit black and white images. This procedure rules out confounding shapes due to overlapping of various colors, where overlapping polychromatism brings additional noise associated both with intense DAPI or H&E staining. The compression of staining applied to plain polychromatic images results in a grey scale, which was implemented by enhanced image contrast, thus allowing cells and nuclei to be visualized as white objects with enhanced definition of cell/nuclear borders. Slices were constantly analyzed at 20X magnification, and the count was performed on 4 random areas (each measuring 200 μm^2).

Three slices from each retina were stained with DAPI to quantify nuclei within ONL, INL, RPE, and GCL layers. Counts of DAPI-positive nuclei in ONL and INL was carried out by using the same procedure described for H&E-stained slices to sort cell/nuclear density within 4 random areas (each measuring 200 μm^2). Within RPE and GCL, due to the placement of cells as a monolayer, without overlapping structures, cell nuclei were counted with no need of image transformation along a length of 450 µm, which was used as a linear reference.

In summary, this procedure allows to overcome the most critical caveat concerning the count of cell nuclei within ONL and INL, where extreme cell packaging occurs. Therefore, following 8-bit conversion, white DAPI-stained nuclei were counted following a cut-off that was established by modifying contrast and brightness. In this way, the natural image captured at light microscopy was homogeneously altered to enhance well-stained structures while suppressing faint staining. This polishing despite altering original data provides an esteem of well-stained cells and nuclei. This was achieved by setting contrast and brightness of primary light microscopy pictures at +77 and +24, respectively, when analyzing DAPI-stained structures. Contrast and brightness of black and white transformed H&E-stained slices were +77 and +112, respectively. This image arrangement was applied uniformly to each area from each slice from both groups and it was carried out by selecting the black and white (greyscale) option and selecting these specific values for contrast and brightness. The effects of this software application led to improve clear-cut identification of cell/nuclear contours. Thus, only frankly stained structures are visualized and can be easily counted, while faintly stained structures are cut off leading to negligible, barely stained structures. In the grey (black and white) tonal channel the input selected by such an image transformation corresponds to 0.40 of mean brightness (gamma) in a 0-255 black and white scale of input for both H&E and DAPI. This value of gamma for counting collected images is a compromise allowing to count reliably most nuclei and cells without including confounding patterns. This approach circumvents the variability and cell packaging within the retina which makes it debatable and non-valid the use of non-biased automated stereology on primary images.

In specific retinal layers such as RPE and PRL, altered thickness is critical since it is associated with retinal degeneration. Therefore, the mean thickness of these layers was calculated along 4 different sites from 3 slices from 7 retinas. Results are express as the mean thickness ± SEM per group.

Densitometry analysis of immunoreactivity

Optical density was used as a semi-quantitative parameter by measuring density produced by each specific immunohistochemical analysis (either immunofluorescent or immunoperoxidase staining). Again, data were collected in each slice from 200 μm^2 random areas concerning ONL and INL or 450 µm lines for RPE and GCL. Images from each slice were acquired at 20X magnification on 3 stained slices, sampled at 100 µm interval for each animal ($N=7$ per group).

Analysis of the length of fluorescent structures

As reported above, when establishing the integrity of RPE, the occurrence of immunostaining for specific RPE markers (RPE65, ZO1, and occludin) was assessed by measuring the length of immunoreactive segments for each marker. The length of continuous immunostaining was also measured for LC3 and alpha-syn within RPE. Images acquired at 20X magnification on 3 stained slices, sampled at 100 µm interval for each animal ($N=7$ per group) were used for the analysis. Quantification was carried out by measuring the length of immunoreactive linear extent, which was expressed in µm.

Data were reported as the mean ± SEM. Statistical analysis was carried out by using GraphPad Prism Software. Group comparison was carried out by using unpaired two-tailed Student's *t*-test. Again, Student's *t*-test may have not covered the essence of the biological distribution of variance. Therefore, One-Way ANOVA was used in addition. The null hypothesis (H_0) was rejected for p-values < 0.05.

Results

Heterozygosity for *BECN1* decreases both primary transcript and protein expression in the whole eyeball

As shown in Fig. 1a, the amount of the primary RNA transcript BECN1 of the *BECN1* gene, that was measured through real time polymerase chain reaction (RT-PCR), decreased more than 50% in BECN+/- compared with WT mice (0.56 ± 0.10 compared with 1.34 ± 0.24). In line with this, when the Beclin1 protein amount was measured at western blotting (representative blot of Fig. 1b, and graph of Fig. 1c), a similar decrease was calculated concerning semiquantitative measurement of optical density of the Beclin1 protein (0.43 ± 0.08 compared with 1 ± 0.28). The housekeeping protein for western blotting, vinculin, was selected for two main reasons: (i) the molecular weight of Beclin1, which allows to visualize in the same run both proteins; (ii) to rule out the bias that, reduced Beclin1 might alter the expression of autophagy-dependent housekeeping proteins but vinculin. The uncropped gels for western blotting are included as Supplementary Information. These data refer to the whole eyeball including the choroid and sclera. These data indicate that BECN+/- mice do express levels of the primary transcript and protein amount (roughly 50% of WT) as expected from silencing one *BECN1* allele.

Heterozygosity for *BECN1* differentially affects various retinal layers

As shown in representative Fig. 2 heterozygosity for *BECN1* leads to a decrease of Beclin1 immunostaining, which is measured in the graph of Fig. 2b and h. As evident from the representative figures and the graphs reporting the staining in each retinal layer, the decrease in Beclin1 immunostaining variably affects each retinal layer (representative pictures and cartoon of Fig. 2a and graphs of Fig. 2b and h). For instance, GCL undergoes a dramatic suppression of Beclin1 immunostaining in BECN+/- mice, where negligible ganglionic cells appear to be stained with anti-Beclin1 antibodies Fig. 2a, graph of Fig. 2b. In contrast, the IPL is not significantly affected by the expression of the protein Beclin1 concerning staining intensity, although the thickness of this layer appears to be increased (Fig. 2a and graph of Fig. 2c). Moving towards outer layers, the INL is markedly reduced concerning the density of Beclin1 immunostaining (Fig. 2 and graph of Fig. 2d) in BECN+/- mice compared with WT. A slight decrease, though significant, is detectable in the immunostaining of OPL in BECN+/- compared with

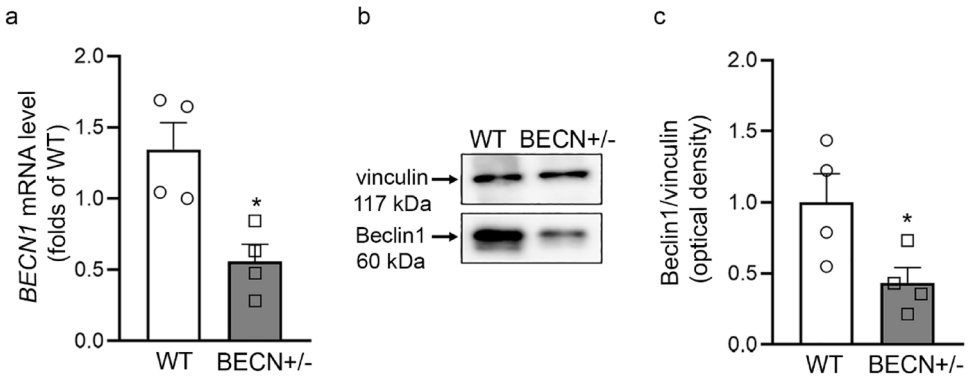

Fig. 1 *BECN1* heterozygosity decreases both *BECN1* primary RNA transcript and Beclin1 protein expression in the whole eyeball. **a** Graph reports RTqPCR quantification of *BECN1* mRNA levels ($N=4$ for each experimental groups). **b** Representative western blotting for Beclin1. **c** Graph reports the ratios between Beclin1 protein and the housekeeping protein vinculin. Values are reported as the means ± SEM ($N=4$ for each experimental groups). Group comparison was carried out by using unpaired two-tailed Student's *t*-test, and One-Way ANOVA with Sheffe's post-hoc analysis. The null hypothesis (H0) was rejected for p-values < 0.05

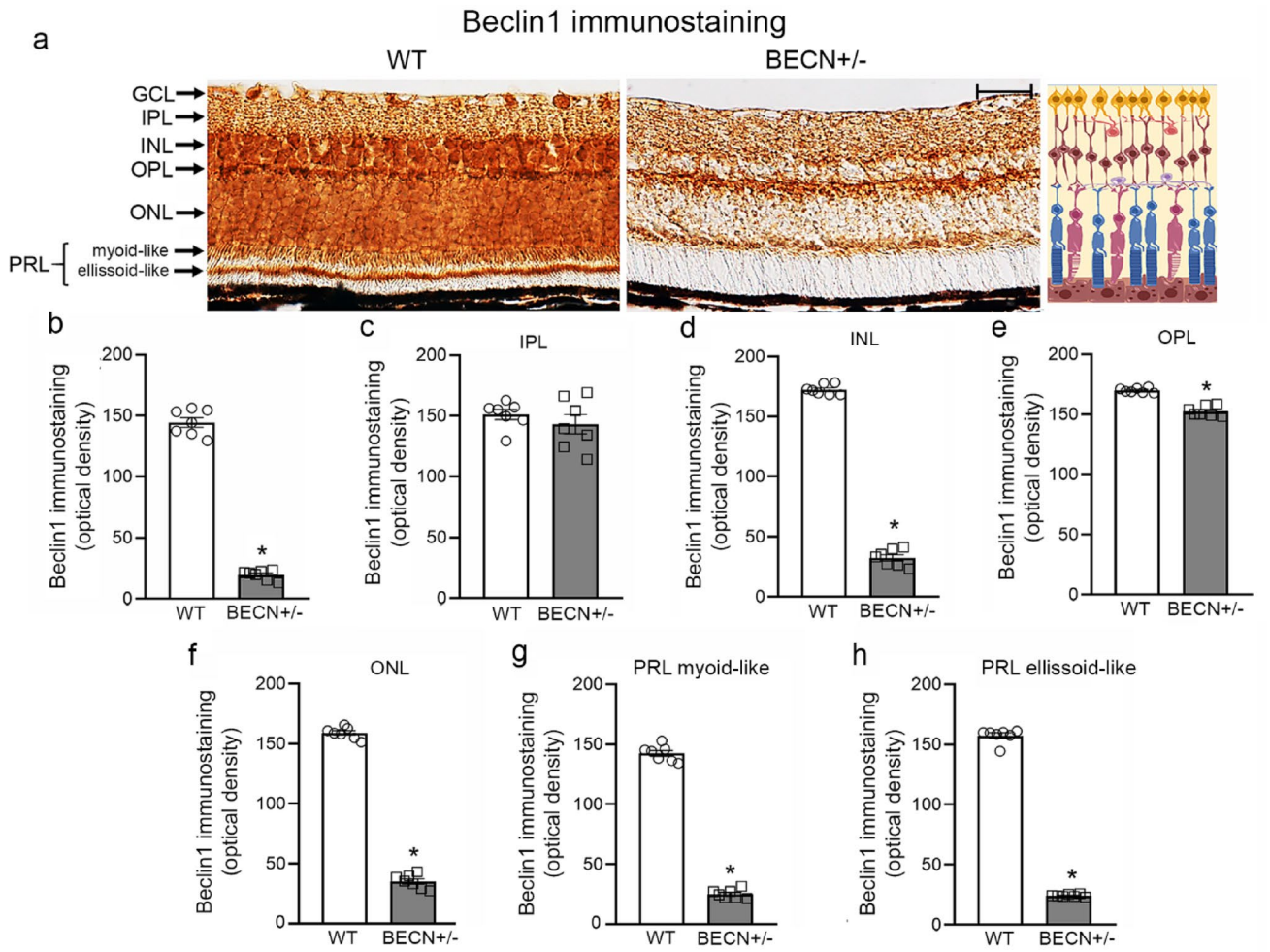

Fig. 2 Heterozygosity for *BECN1* leads to layer-specific suppression of Beclin1 immunohistochemistry. **a** Representative images showing Beclin1 immunohistochemistry in the whole retina from WT and BECN+/- mouse. On the left abbreviations used for identifying some retinal layers are reported: *GCL* ganglion cell layer, *IPL* inner plexiform layer, *INL* inner nuclear layer, *OPL* outer plexiform layer, *ONL* outer nuclear layer, *PRL* photoreceptor layer which includes the myoid- and ellissoid-like segments. The cartoon on the right reports a scheme corresponding to these retinal layers. A marked variability in Beclin1 immunostaining is evident between WT and BECN+/- mice and across various retinal layers from each group. Graphs **b**–**h** report densitometry of Beclin1 immunostaining in specific retinal layers from each group. Values report optical density expressed as the means ± SEM ($N = 7$ per group). Group comparison was carried out by using unpaired two-tailed Student's *t*-test, and One-Way ANOVA with Sheffe's post-hoc analysis. The null hypothesis (H0) was rejected for p-values < 0.05. **a** Scale bar = 50 µm

WT (Fig. 2a and graph of Fig. 2e). Again, in the ONL a severe suppression of Beclin1 immunostaining is measured (Fig. 2a and graph of Fig. 2f).

The PRL of WT mice, is partly stained for Beclin1 at the level where the outer photoreceptor connects with inner photoreceptor segment likely corresponding to myoid and ellissoid (myoid-like and ellissoid-like PRL in the picture). This stained segment of PRL from WT become pale in BECN+/- mice (Fig. 2a and graphs of Fig. 2g and h, respectively). The rest of PRL and likely the area corresponding to the POS is pale in both groups of mice (Fig. 2a). The immunoperoxidase within RPE cannot be detected although the thickness of the melanin layer corresponding to RPE appear to be reduced in BECN+/- mice. To check reliably the integrity of RPE, immunofluorescence against specific RPE antigens was used instead.

Heterozygosity for *BECN1* differentially affects cell viability within various retinal layers

To provide a plain view of all retina layers in WT and BECN+/- mice pictures of H&E-stained whole retina is provided (representative Figs. 3 and 4, respectively). Here each retinal layer can be easily recognized with the aid of a cartoon placed aside. In WT plain H&E histochemistry allows to document the integrity of each retinal layer owing high cell density (Fig. 3). When a comparable representative picture is taken from a BECN+/- mouse retinal integrity is

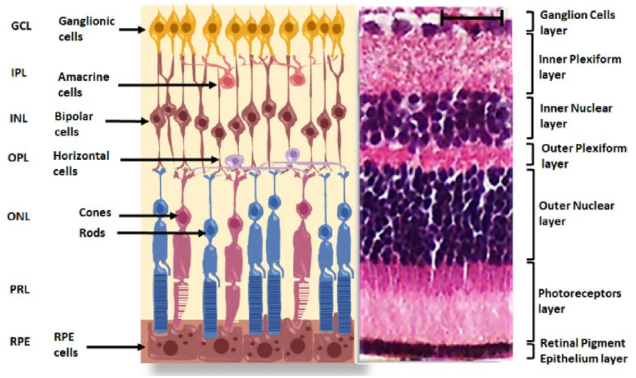

Fig. 3 Cartoon and representative H&E histochemistry of the whole retina from a WT mouse. On the left a cartoon of the retina is reported where each layer is indicated along with its abbreviation and the specific cell type. On the right, representative H&E histochemistry from the retina of WT mice allows to appreciate the integrity and cellular density of each retinal layer. In detail, H&E staining allows to distinguish architecture of each retinal layers, including those areas owing a high cellular density (INL and ONL). Scale bar = 50 µm

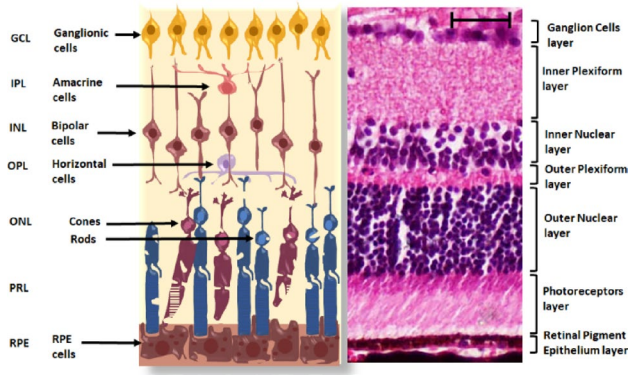

Fig. 4 Cartoon and representative H&E histochemistry of the whole retina from BECN+/- mouse. On the left the cartoon of the retina replicates that reported in Fig. 3. On the right, representative H&E histochemistry from the retina of BECN+/- mouse provides evidence of altered layer integrity and cellular morphology. In detail, a deficiency of Beclin1 leads to dramatic alterations concerning cell density and layers' morphology. Scale bar = 50 µm

lost in most layers where cell density appears to be markedly reduced and cell types show abnormal morphology, as symbolized in the cartoon (Fig. 4). This is magnified in Fig. 5, where specific retinal layers are shown in representative pictures of Fig. 5a. In detail, when H&E histochemistry is carried out, the heterozygous expression of Beclin1 leads to a frank cell loss, which appears to be mostly evident concerning INL and ONL (Fig. 5a and graphs of Fig. 5b and c). The decreased cell density of ONL and INL is well-appreciated in representative pictures of Fig. 5a where the H&E staining is provided along with its conversion to black and white (8-bit) images (from WT and BECN+/- mice). These representative pictures serve also as a reference to show how cell count is much more feasible in densely packed retinal layer following 8-bit inversion and conversion (as explained in the statistics). The cell counts of INL and ONL is reported as cell density in the graphs of Fig. 5b and c. These graphs report a severe cell loss of both bipolar cells counted within INL (16.86 ± 1.57 cells in 200 µm^2 counted WT compared with 9.57 ± 1.39 cells in 200 µm^2 counted in BECN+/- mice, graph of Fig. 5b) and a similar loss of rods and cones within ONL (34.05 ± 2.16 cells in 200 µm^2 counted in ONL of WT compared with 23.71 ± 2.06 cells in 200 µm^2 counted in BECN+/- mice, graph of Fig. 5c). No severe alteration can be documented concerning the OPL and IPL, as shown in representative pictures of Fig. 5a.

Cell degeneration was documented by a derangement and loss of photoreceptors, as witnessed by a reduced thickness PRL. In detail, the PRL, containing the outer segment of photoreceptor, appears to be deranged in BECN+/- mice, with empty areas. These are compatible with amorphous deposition as in pseudo-drusen (representative pictures of Fig. 5a). This appearance suggests atrophy of the outer segment of photoreceptors as measured by the graph of Fig. 5d reporting a decreased thickness of PRL (68.43 ± 6.02 µm in WT compared with 42.57 ± 3.64 µm counted in BECN+/- mice). Such an atrophy is even more severe concerning the RPE which is reduced by almost 50% in thickness considering the marked melanin layer (10.29 ± 1.60 in WT compared with 5.58 ± 1.27 µm counted in BECN+/- mice, graph of Fig. 5e). Still, the deleterious effects on BECN+/- RPE is more evident by using immunostaining for specific RPE antigens. Concerning the GCL, in BECN+/- mice the cell phenotype does not appear to be noticeably altered following H&E (representative pictures of Fig. 5a). This contrasts with the marked difference concerning Beclin1 immunostaining which was almost absent in GCL of BECN+/- mice (representative Fig. 2a, and graph in Fig. 2b).

Such a strong decrease of Beclin1 immunostaining observed in GCL could be related to a reduced size of GCL nuclei observed in BECN+/- mice following DAPI histofluorescence as reported in Fig. 6a and graph of Fig. 6b. As reported, the number of ganglionic cell nuclei was slightly, though significantly decreased in BECN+/- mice (102.14 ± 6.46 nuclei in 450 linear µm counted in wild types compared with 89.21 ± 4.24 nuclei in 450 linear µm counted in BECN+/- mice, representative Fig. 6a and graph of Fig. 6b).

As evidenced in representative pictures of Fig. 6a following DAPI histofluorescence, the effects of BECN1+/- on cell viability are confirmed by a massive decrease of neuronal nuclei in INL (16.43 ± 1.71 nuclei in 200 µm^2 counted in wild types compared with 9.28 ± 1.59 nuclei in 200 µm^2 counted in BECN+/- mice, representative Fig. 6a and graph of Fig. 6c) and ONL (29.86 ± 0.73 nuclei in 200 µm^2 counted in WT compared with 22.43 ± 1.71 nuclei in 200

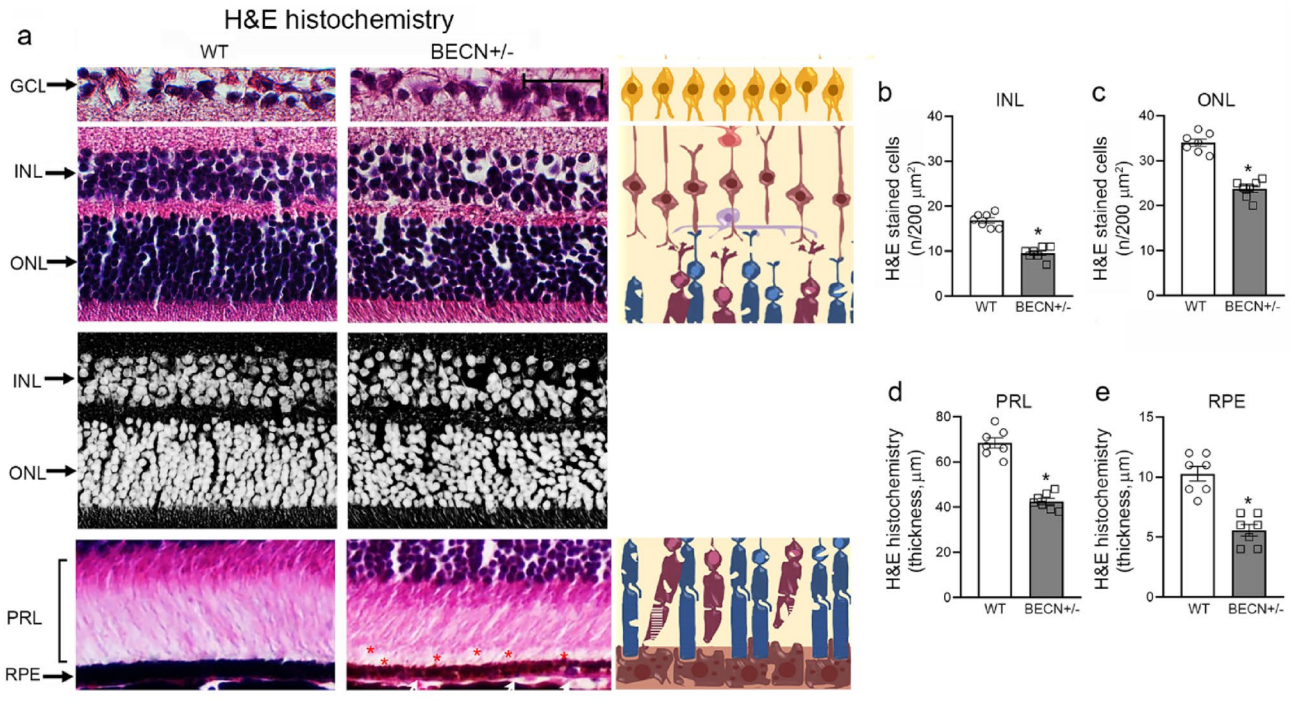

Fig. 5 In BECN+/- mice H&E-stained retinal layers are altered. **a** On the left representative H&E stained representative slices from a WT and BECN+/- mouse indicate severe layer-dependent morphological alterations summarized in the cartoon on the right. The black and white images represent the 8-bit converted/inverted transformation allowing cell count as reported in Materials and Methods. Graphs (**b**–**c**) report the decrease in the cell number (mostly evident for INL and ONL) and graphs (**d**–**e**) report the decrease in layer thickness (mostly evident for PRL and RPE) measured in BECN+/- compared with WT mice. Values are the means ± SEM ($N = 7$ per group). Group comparison was carried out by using unpaired two-tailed Student's *t*-test, and One-Way ANOVA with Sheffe's post-hoc analysis. The null hypothesis (H0) was rejected for *p*-values < 0.05. Scale bar = 50 µm

µm^2 counted in BECN+/- mice, representative Fig. 6a and graph of Fig. 6d).

By profiting of histofluorescence the count of RPE cell nuclei was feasible following DAPI. This count confirms what was inferred by observing the melanin thickness in Fig. 5a), in detail a thinning of RPE is accompanied by a frank loss of RPE cell nuclei (42.71 ± 3.72 nuclei in 450 linear µm counted in WT compared with 28.29 ± 1.80 nuclei in 450 linear µm counted in BECN+/- mice, representative Fig. 6a and graph of Fig. 6e).

Heterozygosity for *BECN1* alters the amount and phenotype of RPE cells

As reported in representative pictures, and cartoon of Fig. 7a, and the graph of Fig. 7b specific RPE immunostaining for the protein RPE65 indicates a dramatic suppression of stained cells in BECN+/- mice (508.86 ± 5.78 µm of continuous fluorescent length in WT compared with 85.01 ± 12.91 µm counted in BECN+/- mice, representative Fig. 7a and graph of Fig. 7b). Since the outer segments of rods and cones are embraced by cell processes of RPE cells, it is it is likely that reduced RPE65 immunostaining, may extend to the PRL which includes POS. This is in line with the effects of RPE65, which is actively involved in the phagocytosis of POS by RPE cells (Zhang et al. 2018). In connection with RPE65, it is demonstrated that Beclin1 plays a critical role in such a process by fostering the endocytosis of photoreceptors within RPE cells. Thus, it is not surprising that a partial deficiency of Beclin1 affects the presence of RPE65 and it is likely to impair its shuttling towards photoreceptors (Zhang et al. 2018). This may explain the different pattern of immunostaining which is evident in representative Fig. 7a. A hallmark of RPE integrity is routinely represented by the tight junction protein ZO1. Therefore, immunostaining for ZO1 is commonly used to assess viability of RPE, while its early alteration during AMD and retinal degeneration witnesses for RPE degeneration.

As reported in representative pictures of Fig. 8a, in BECN+/- mice a marked loss of ZO1 immunostaining within RPE is documented. This is evident in representative pictures of Fig. 8a.

Apart from being a pathological culprit of RPE cell loss, a decrease in ZO1 immunostaining witnesses for a loss of the seminal role of RPE in constituting the blood-retinal barrier (Georgiadis et al. 2010). It is intriguing that in

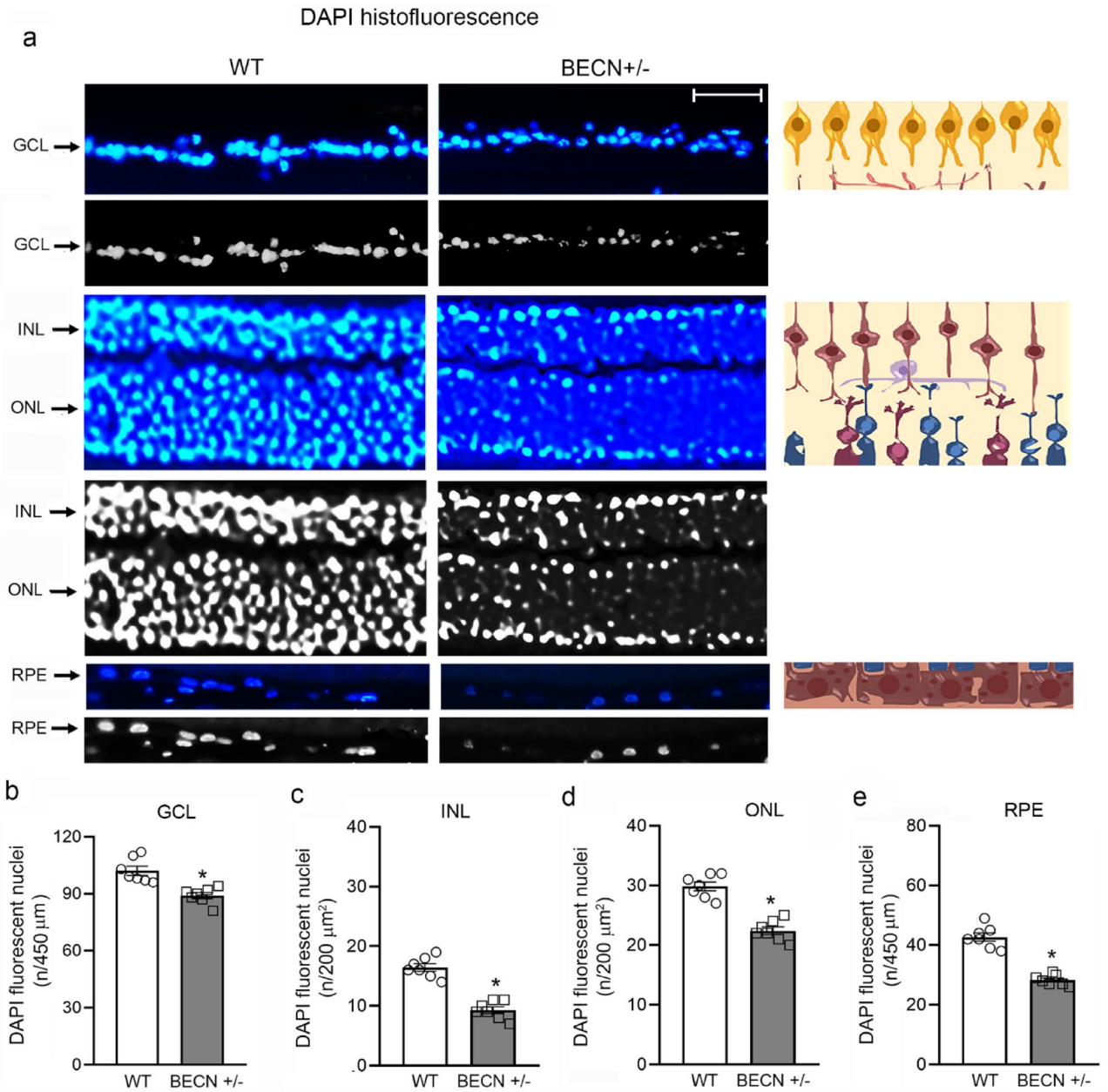

Fig. 6 In BECN+/- mice DAPI-stained retinal layers are altered. **a** On the left representative DAPI-stained representative slices from a WT and BECN+/- mouse indicate severe layer-dependent morphological alterations summarized in the cartoon on the right. In detail, nuclear count following DAPI stained and enabled by 8-bit converted/inverted transformation shows a significant layer-dependent nuclear loss. This is expressed by nuclear counts reported in the graphs (**b**–**e**) indicating a slight nuclear loss in the GCL and a severe effect within INL, ONL and RPE occurring in BECN+/- compared with WT mice. Values are reported as the means ± SEM ($N = 7$ per group). Group comparison was carried out by using unpaired two-tailed Student's *t*-test, and One-Way ANOVA with Sheffe's post-hoc analysis. The null hypothesis (H0) was rejected for p-values < 0.05. Scale Bar = 50 µm

BECN+/- mice the loss of ZO1 is documented both within RPE and above, at the level of the outer segment of photoreceptors (POS), where the cell processes of RPE cells extend.

This explains why when ZO1 immunostaining is calculated in the PRL such a decrease is still significant (95.67 ± 1.34 in WT compared with 66.10 ± 1.43 in BECN+/- mice, graph of Fig. 8b).

Nonetheless, the severe loss of ZO1 is mostly evident within RPE (509.57 ± 1.52 µm of continuous immunofluorescent length in WT compared with 99.57 ± 2.73 µm counted in BECN+/- mice, graph of Fig. 8c). This effect is comparable with the marked decrease of RPE65 immunostaining.

To further validate the impairment of the tight junctions within RPE in BECN+/- mice another RPE marker, occludin,

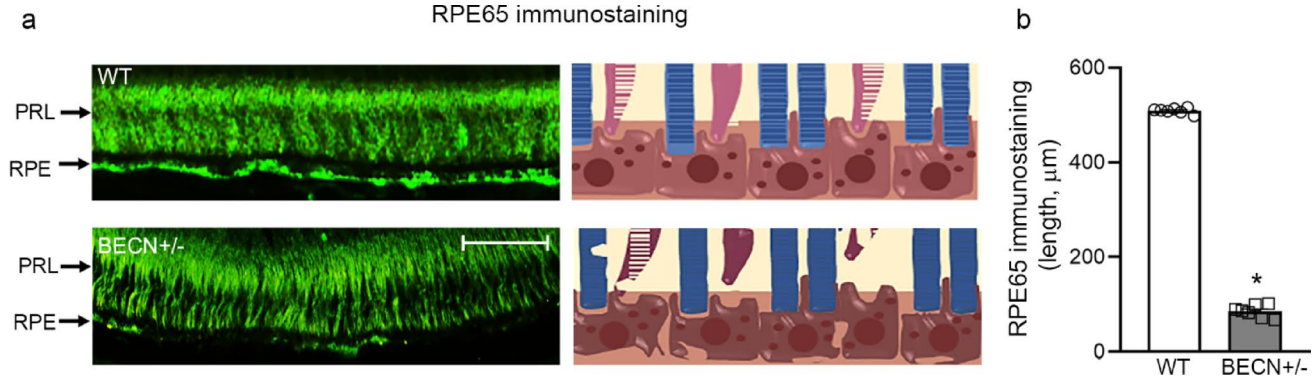

Fig. 7 In BECN+/- mice RPE65 protein expression is reduced. Representative images of RPE65 immunostaining in PRL and RPE layer from BECN+/- and WT mice. A schematic cartoon showing the PRL and RPE is reported on the right of the panel. **b** Graph reports the length of immunostaining for RPE65 which was continuous and homogeneous in WT while it was dramatically reduced in BECN+/- mice. Representative images shown in (**a**) allow to appreciate that altered expression of RPE65 also involves the overlying photoreceptors within the PRL layer, although such an altered pattern does not correspond to a specific decrease in protein amount. Values are means ± SEM ($N = 7$ per group). Group comparison was carried out by using unpaired two-tailed Student's *t*-test, and One-Way ANOVA with Sheffe's post-hoc analysis. The null hypothesis (H0) was rejected for p-values < 0.05. **a** Scale Bar = 50 µm

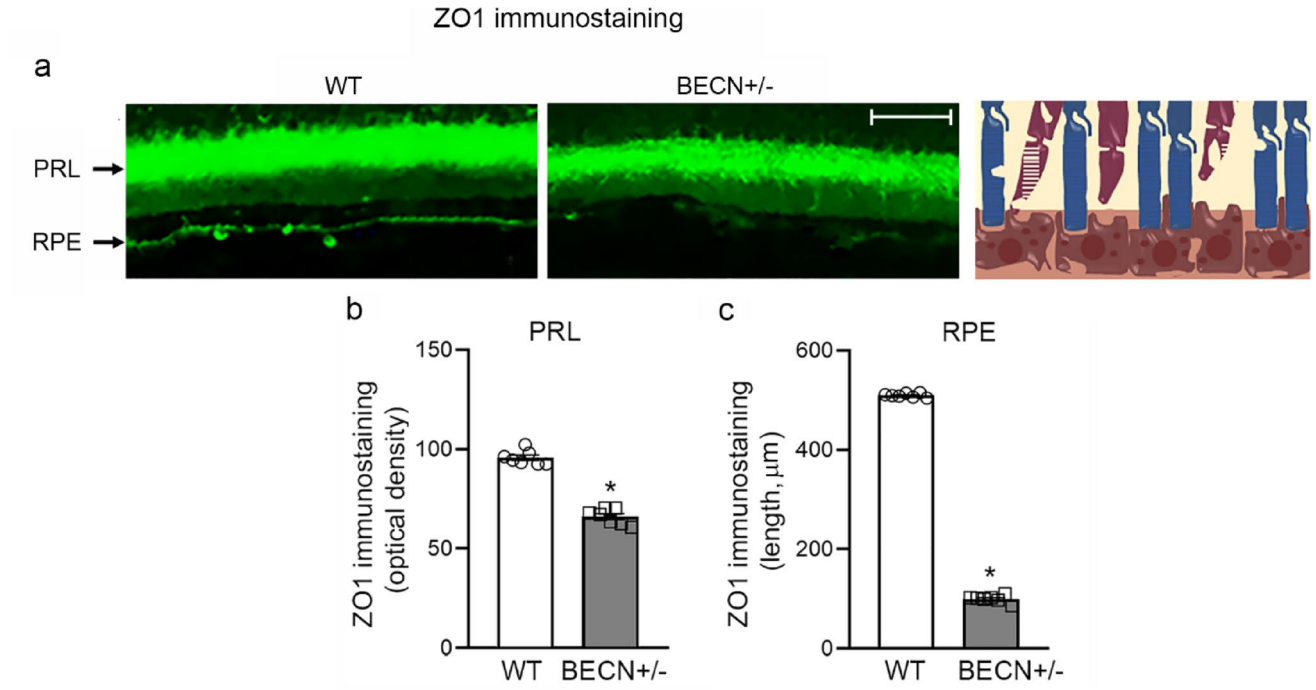

Fig. 8 In BECN+/- mice ZO1 protein expression is reduced in PRL and RPE. Representative images of ZO1 immunostaining in RPE and PRL layers of BECN+/- and WT mice are shown in (**a**). On the right of the panel a cartoon provides a schematic representation of RPE and PRL layers. Densitometry quantification of ZO1 immunofluorescence at optical density in PRL and the length of ZO1 immunostaining within RPE are reported in graphs (**b**) and (**c**), respectively. Values are given as the means ± SEM ($N = 7$ per group). Group comparison was carried out by using unpaired two-tailed Student's *t*-test, and One-Way ANOVA with Sheffe's post-hoc analysis. The null hypothesis (H0) was rejected for p-values < 0.05. Scale Bar = 50 µm

was tested (representative pictures of Fig. 9a). Again, the continuous linear staining of occludin-positive RPE cells, which is visible in WT mice is lost following depletion of one *BECN1* allele (510.71 ± 1.76 in WT compared with 107.43 ± 2.33 in BECN+/- mice, graph of Fig. 9b). As reported for RPE65, a different pattern of immunostaining appears in representative Fig. 9a concerning PRL. As reported for RPE65 the immunostaining of PRL for occludin shifts towards a patchy pattern in BECN+/- compared with a more homogeneous staining of WT.

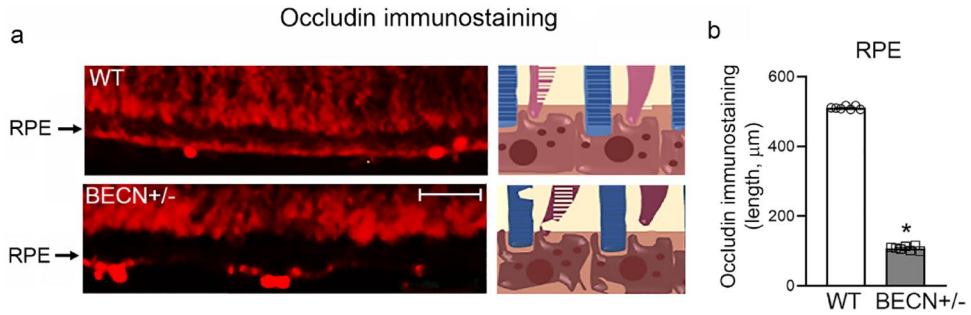

Fig. 9 In BECN+/- mice occludin protein expression is reduced in RPE. **a** Representative images of occludin immunostaining in RPE layer of WT and BECN+/- mice. The representative image of occludin immunofluorescence clearly shows a dramatic decrease in BECN+/- compared with WT mice. In the PRL of BECN+/- mice the pattern of occludin expression is modified compared with WT, although a change in the amount of immunofluorescence is debatable in PRL. A schematic cartoon showing RPE is reported on the right of the panel. Quantification of continuous length of occludin immunofluorescence within RPE of WT and BECN+/- mice is reported in graph (**b**). Values are given as the means ± SEM ($N = 7$ per group). Group comparison was carried out by using unpaired two-tailed Student's *t*-test, and One-Way ANOVA with Sheffe's post-hoc analysis. The null hypothesis (H0) was rejected for p-values < 0.05. Scale bar = 50 µm

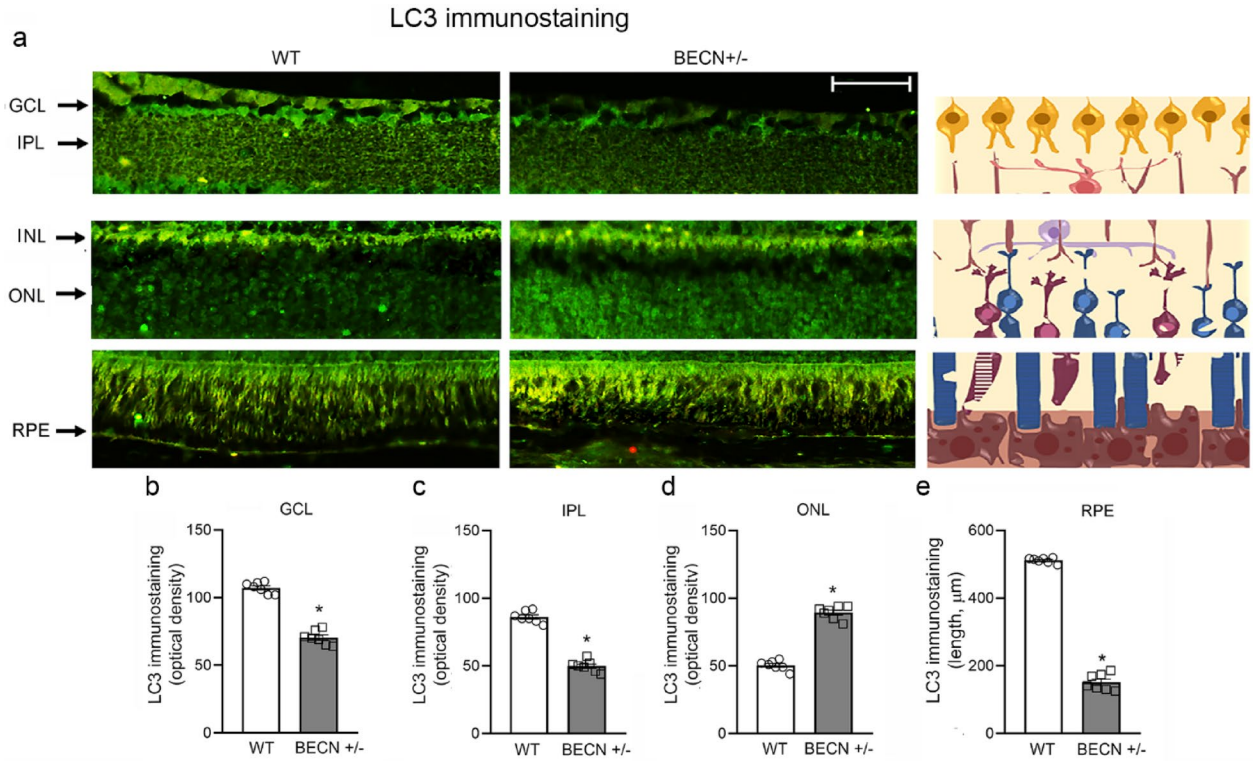

Fig. 10 In BECN+/- mice the expression of microtubule-associated protein 1 A/1B-light chain 3 (LC3) is altered within various retinal layers. **a** Representative images of LC3 immunostaining in GCL, IPL, ONL, RPE of BECN+/- and WT mice. On the right of the panel schematic cartoons report these retinal layers. Optical density (GCL, IPL, ONL) and length (RPE) of LC3 immunofluorescence are reported in graph (**b**–**e**). Values are given as the means ± SEM ($N = 7$ per group). Group comparison was carried out by using unpaired two-tailed Student's *t*-test, and One-Way ANOVA with Sheffe's post-hoc analysis. The null hypothesis (H0) was rejected for p-values < 0.05. Scale bar = 50 µm

Heterozygosity for *BECN1* alters the amount and distribution of other autophagy-related proteins

To assess a potential alteration of other autophagy-related proteins such as LC3 and LAMP1 because of reduced Beclin1 expression, specific immunostaining for these proteins was carried out. In fact, LC3 is routinely considered to initiate autophagy as much as Beclin1, and the expression of LC3 may potentially compensate for a Beclin1 deficiency. Unexpectedly, as reported in representative pictures of Fig. 10a, the amount of LC3 was rather decreased in most retinal layers, starting from GCL

(Fig. 10a and graph of Fig. 10b). In detail, optical density of GCL was 107.30 ± 1.55 in WT compared with 70.43 ± 1.96 in BECN+/- mice, graph of Fig. 10b. Similarly, a significant decrease was visible within IPL (Fig. 10a) where LC3 immunostaining is decreased (86.14 ± 1.61 in WT compared with 49.86 ± 1.59 in BECN+/- mice) as reported in the graph 10c. No significant effect was detectable below IPL, within INL where no LC3 immunostaining was noticeable neither in WT not in BECN+/- mice (Fig. 10a). Proceeding further towards the external retina, an inversion took place, where the amount of LC3 was increased within ONL of BECN+/- mice compared with WT (Fig. 10a). In detail, optical density of LC3 immunofluorescence within ONL is 50.43 ± 1.34 in WT compared with 89.43 ± 1.83 in BECN+/- mice (graph of Fig. 10d).

In the outer retina, the amount of LC3 immunostaining changes the topographical pattern within PRL and is markedly reduced within RPE cells. In detail, the linear extent of immunostaining for LC3 was reduced in RPE of BECN+/- mice (Fig. 10a and graph of Fig. 10e). Such a decrease is likely to be induced to the actual loss of RPE cells observed in BECN+/- mice (graph of Fig. 5e which roughly correspond to the decrease measured in the graph of Fig. 10e). The length of LC3 immunofluorescence within RPE is 511.90 ± 2.92 µm in WT compared with 151.31 ± 9.23 µm in BECN+/- mice (graph of Fig. 10e).

The progression of the autophagy clearance towards lysosome is expected to be associated with the expression of LAMP1. The amount of LAMP1 immunostaining undergoes a specific increase in the outer retina/inner choroid (as shown in representative pictures of Fig. 11a). At the level of RPE a widespread staining is present, which extends just beneath RPE cells. The increase of immunofluorescence

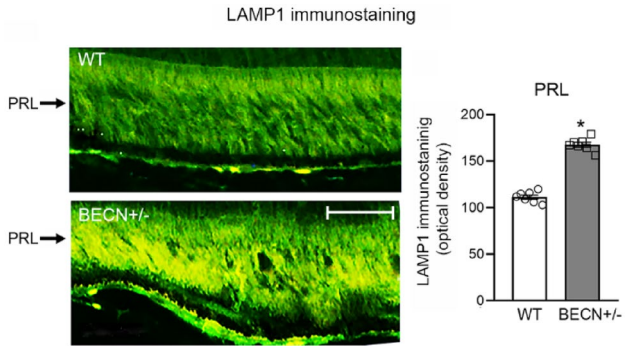

Fig. 11 In BECN+/- mice the expression of lysosome-associated membrane protein 1 (LAMP1) is increased within PRL layer. **a** Representative images of LAMP1 immunostaining in PRL layer of BECN+/- and WT mice. Densitometric analysis of optical density for LAMP1 immunofluorescence in PRL layer of BECN+/- and WT mice is shown in (**b**). Values are given as the means ± SEM ($N = 7$ per group). Group comparison was carried out by using unpaired two-tailed Student's *t*-test, and One-Way ANOVA with Sheffe's post-hoc analysis. The null hypothesis (H0) was rejected for p-values < 0.05. Scale bar = 50 µm

concerned intensity, area, thickness and continuity. Such a strong increase in the outer retina may depend on the accumulation of lysosomes above and below RPE which may be due to a defect in the autophagy progression and accumulation of drusen/pseudo-drusen-like structures which may be related to the increased density of PRL (112.05 ± 2.26 in WT compared with 170.96 ± 3.68 in BECN+/- mice, graph of Fig. 11b).

This is in line with the amount of staining for lipids, which is observed following red oil histochemistry (representative pictures of Fig. 12a–c), which is more evident in BECN+/- mice at the level of RPE and just above, within the POS or below the RPE, in the inner choroid. This suggests the deposition of lipid-rich amorphous material, consistent with drusen formation in the outer retina of BECN+/- mice.

In Fig. 12 the irregularity and reddish color of POS appears discontinuous in BECN+/- compared with continuous, regular and pale color in WT mice. In BECN+/- the reddish tone overlaps with melanin in the RPE and below, in the thickened choroid. This is evident at increasing magnification progressively, from Fig. 12a–c.

Alpha-syn immunostaining

As shown in the panoramic view of the all retina of representative Fig. 13a, the outer retina from BECN+/- mice features a decrease alpha-syn immunostaining compared with WT mice, this is reversed in the inner retina. At this level, an increased alpha-syn immunostaining is noticeable within IPL and INL of BECN+/- compared with WT mice (representative Fig. 13b and graphs of Fig. 13d and e). In detail, within IPL the density of alpha-syn immunostaining is 21.57 ± 1.17 in WT compared with 40.14 ± 1.18 in BECN+/- mice (Fig. 13d), while in the INL density is 26.92 ± 1.56 in WT compared with 59.06 ± 0.81 in BECN+/- mice (Fig. 13e). This effect is still evident within most PRL (representative Fig. 13c and graph of Fig. 13f). In contrast, alpha-syn immunostaining is negligible within RPE cells of BECN+/- compared with WT mice (representative Fig. 13c and graph of Fig. 13g). Within RPE, the linear immunostaining for alpha-syn was 506.43 ± 3.82 µm in WT compared with 81.43 ± 4.53 µm in BECN+/- mice (graph of Fig. 13g). In summary, the increase of alpha-syn is remarkable within inner retina of BECN+/- mice. This is reported during maladaptive plasticity which occurs downstream in the inner retina following a damage in the outer retina (Pfeiffer et al. 2020a, b, c).

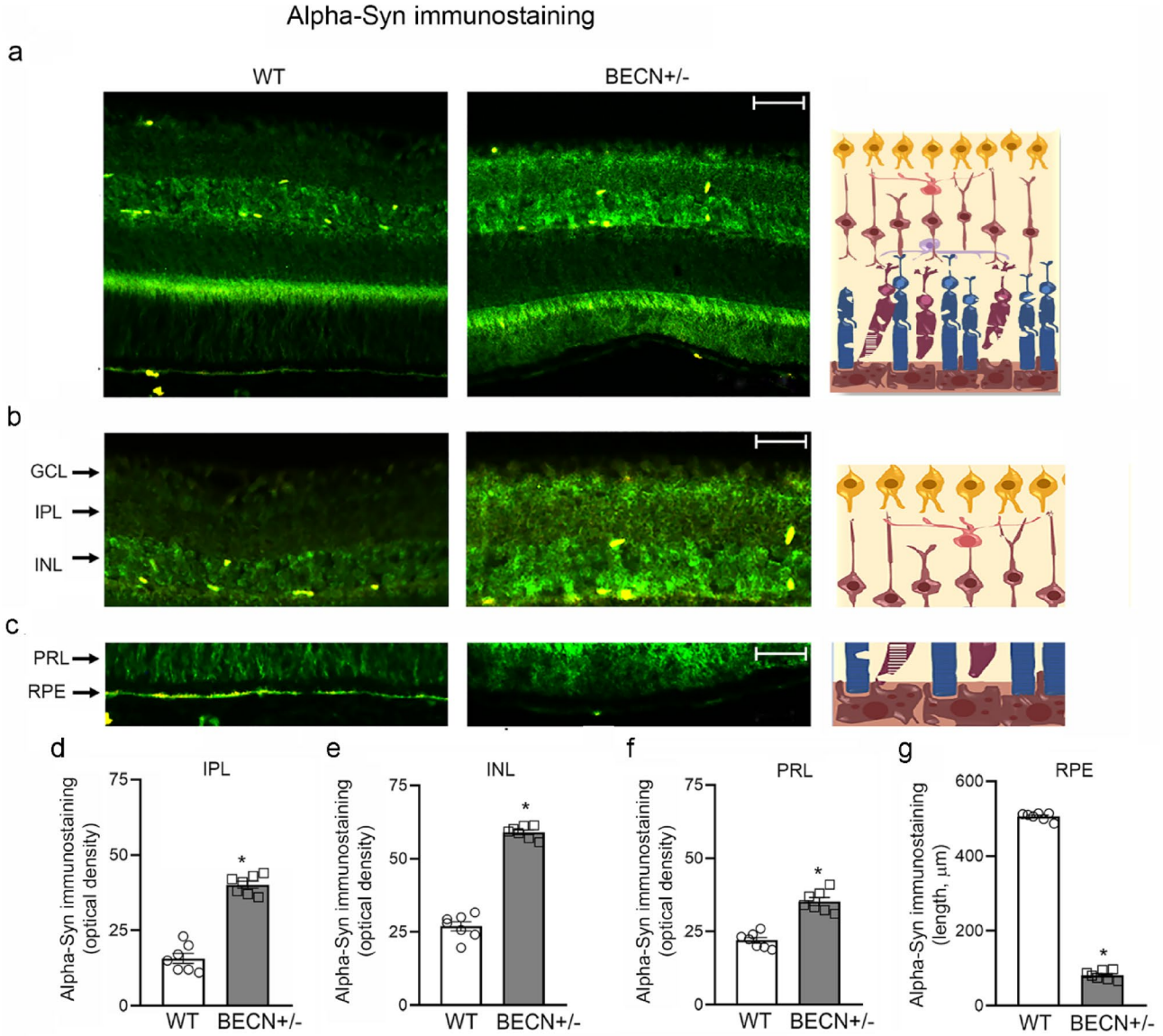

Fig. 12 In BECN+/- mice lipids increase within RPE and PRL layers. Representative images of red oil histochemistry in the whole retina show an increase in BECN+/- compared with WT mice (**a**). Representative images at higher magnification 40X (**b**) and 63X (**c**) of red oil histochemistry suggest that accumulation of lipid material mostly occurs within RPE layer and within PRL, just above the POS segment in the outer retina of BECN+/- compared with WT mice. It is noticeable that irregular and disrupted structure of POS associates with reddish staining, which contrasts with pale PRL observed in WT mice. **a** Scale bar = 100 µm, **b** Scale bar = 50 µm, **c** Scale bar = 25 µm

Discussion

In the present study, the morphology of the retina in aged mice, heterozygous for the gene *BECN1* is analyzed. The relevance of this genetic model applies to the growing role of Beclin1 in the study of retinal disorders mostly produced by retinal degeneration which feature a late onset in the lifespan. This corresponds to the most common retinal degenerative disease, AMD, which indeed is characterized by altered expression of Beclin1 (Kaarniranta et al. 2023). Clinical studies confirm a seminal role of Beclin1 in AMD. In fact, circulating Beclin1 decreases with age in humans and Beclin1 is markedly reduced in patients with AMD (Kubicka-Trzaska et al. 2021). In detail, human patients affected by AMD, have serum levels of Beclin1 which are reduced to less than 10% of levels measured in controls (median, 0.100 ng/ml in AMD patients compared with 1.123 ng/ml of control patients, $p = 0.0033$ as reported in the study of Kubicka-Trzaska et al. 2021). Such a difference is even more pronounced in old patients affected by AMD (Kubicka-Trzaska et al. 2021). In line with a causal effect of a loss of Beclin1 in promoting AMD, and the deleterious effects produced by aging, the present study analyzed the occurrence of retinal degeneration in aged Beclin1 deficient

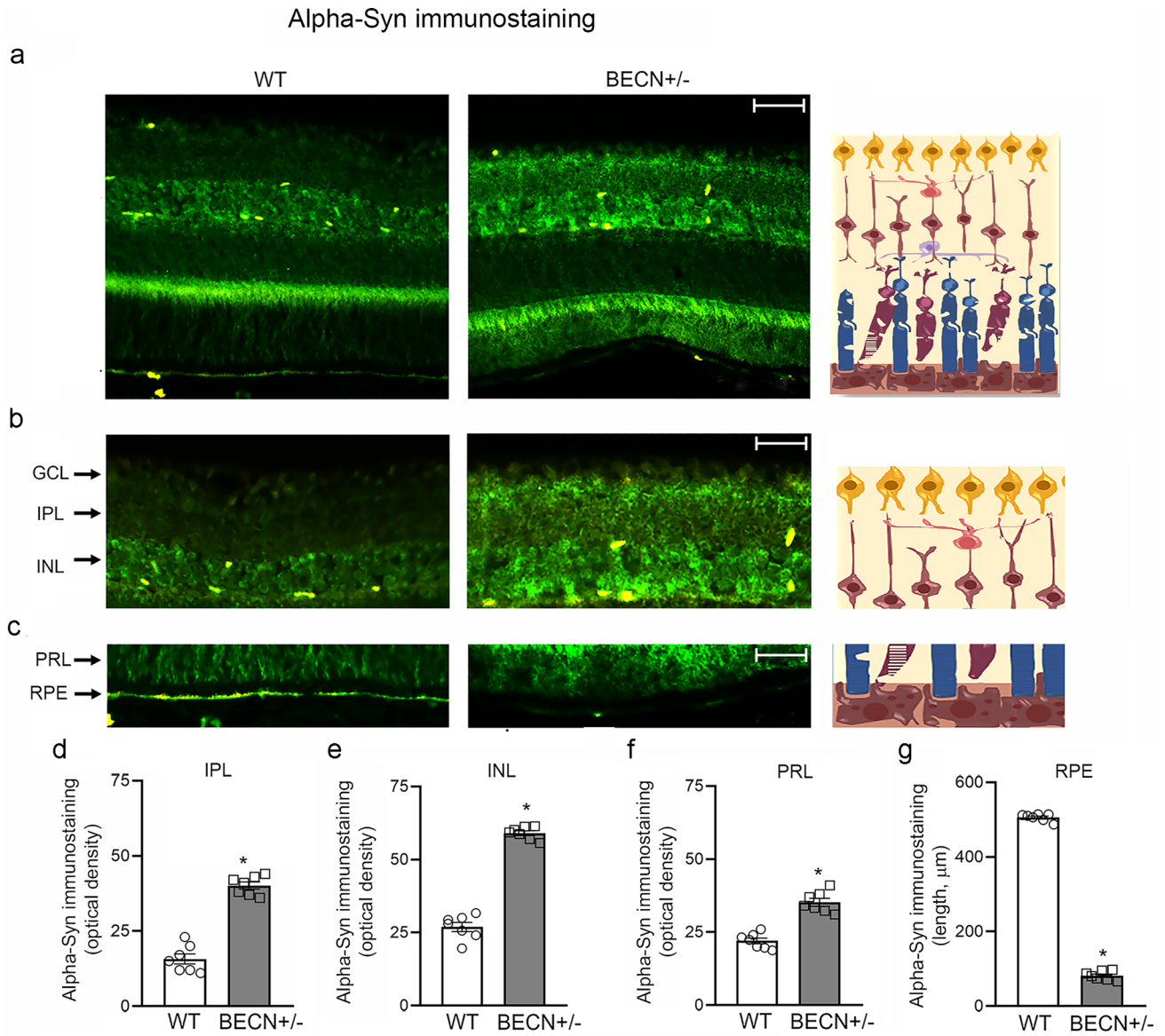

Fig. 13 In BECN+/- mice alpha-syn expression increases within inner retina. Representative images of alpha-syn immunostaining in the whole retina of WT and BECN+/- mice are shown in (**a**) (lower magnification) where the progressive increase of alpha-syn immunofluorescence in the whole retina from a BECN+/- mouse is visible from the RPE towards the inner retina. In representative images (**b**) a higher magnification (40X) shows details of alpha-syn immunostaining within GCL, IPL, INL, while in representative pictures (**c**) alpha-syn immunofluorescence is visible within PRL, and RPE at 40X magnification. On the right of the panel is shown a schematic cartoon with a representation of retinal layers stained in (**b**) and (**c**). Densitometry of immunofluorescence reports a higher alpha-syn immunofluorescence within IPL, and INL in BECN+/- compared with WT mice as reported in graphs (**d**) and (**e**), respectively. Similarly, higher alpha-syn immunofluorescence is detected within PRL from BECN+/- compared with WT mice as reported in graph (**f**). In contrast, alpha-syn immunofluorescence is higher within RPE from WT compared with BECN+/- mice as quantified by measuring the length of immunofluorescence corresponding to the RPE monolayer reported in the graph (**g**). Each value is the means ± SEM ($N = 7$ per group). Group comparison was carried out by using unpaired two-tailed Student's *t*-test, and One-Way ANOVA with Sheffe's post-hoc analysis. The null hypothesis (H0) was rejected for *p*-values < 0.05. **a** Scale bar = 50 µm, **b** Scale bar = 25 µm, **c** Scale bar = 25 µm

mice. The present data indicate that deletion of one allele of the *BECN1* gene in aged mice produces a severe damage to the RPE which further extends to the whole retina. In detail, BECN+/- mice develop a disruption of anatomical continuity of RPE, as typically occurring at early stage in AMD (Jiang et al. 2025). Such damage is associated with a morphological rupture of the outer segment of photoreceptors (POS) which appear to be atrophic and characterized by severe loss of structure. In physiological conditions the connection between RPE and POS is crucial for maintaining the integrity of the outer retina. In detail, RPE cell loss, which is accompanied by a loss of tight junctions between RPE cells

is considered to foster early stages of AMD. In keeping with this, the present study indicates that, in aged BECN+/- mice thinning and cell loss of RPE is concomitant with a defect in key proteins known to be crucial for maintaining tight junctions, which characterize the homeostasis of the outer retina. Such a protein loss is considered as a typical hallmark of AMD (Furuse et al. 1993; Hartsock and Nelson 2008; Pinelli et al. 2025). This is confirmed in the present study in aged BECN+/- mice, where a failure in ZO1 and occludin is documented (Furuse et al. 1993; Hartsock and Nelson 2008). These proteins represent an essential component of the tight junctions between RPE cells and their loss is used in vitro as a hallmark of RPE degeneration (Wolfensberger and Gregor 2010; Molins et al. 2017). The loss of these proteins makes the blood-retinal barrier leaky, which fosters the transitions from dry to wet AMD. In addition, the dismantling of these proteins from the membrane surface of RPE cells is a trigger to induce the epithelial-mesenchimal transitions (EMT), which is key in driving the severity of AMD. In combination to the loss of tight junction proteins, in BECN+/- mice the specific protein RPE65 is suppressed. This protein plays a fundamental role in the turnover of the outer segment of photoreceptors. In detail, RPE65 is expressed by RPE cells, and it is very abundant in the cell processes surrounding the outer segment of photoreceptors (Zhang et al. 2018). Since photoreceptor outer segment is embraced by cell processes of RPE cells, it is likely that altered RPE65 immunostaining, may extend to the photoreceptor layer, which may impair the turnover of the outer segment of photoreceptors. This is consistent with the effects promoted by RPE65, which is actively involved in the phagocytosis of photoreceptor outer segment by RPE cells (Zhang et al. 2018). This autophagy, LC3 mediated phagocytosis (LAP) is deficient in AMD and is fostered by RPE65 which is lost in the present model. In connection with RPE65, it is demonstrated that Beclin1 plays a critical role in such a process including LAP by fostering the endocytosis of photoreceptors within RPE cells. Thus, it is not surprising that a partial deficiency of Beclin1 affects the presence of RPE65 and likely impairs its shuttling towards photoreceptors (Zhang et al. 2018) disrupting POS structure. Damage to RPE cells is essential in the onset of retinal degeneration in the course of AMD. In the present study evidence is provided that in BECN+/- mice RPE is altered concerning the amount of nuclei (stained with DAPI) and the layer continuity (stained with RPE65, ZO1 and occludin). In these mice, RPE undergoes a significant thinning just like occurring in AMD. Moreover, phenotype specific proteins (ZO1, occludin and RPE65) are altered beyond a mere decrease showing an altered pattern of expression, which witnesses for a loss of RPE-generated tight junctions as typically occurring in AMD. Apart from generating a leakage within the blood-retinal barriers, the loss of these proteins also defined as “dismantling” characterizes the typical EMT, which characterize the progression of AMD (Chowdhury et al. 2025; Yang et al. 2026). In fact, in the course of the retinal disease the EMT is a pivot to shift the pathology towards neo-angiogenesis (Liu et al. 2023). This is key in disease worsening when the dry phenotype turns into wet AMD. The tight relationship between RPE and photoreceptors critically depends on the integrity of RPE. Therefore, it is not surprising that a derangement measured here in the RPE cells is associated with thinning and derangement of the outer photoreceptors. This is further justified by the loss of RPE65 in BECN+/- mice which normally regulates the trafficking of aged cell domains of photoreceptors to be phagocytosed by RPE (Zihni 2025; Du and Xia 2025; Markitantova and Simirskii 2025; Etchegaray and Ravichandran 2025).

The occurrence of frank alterations in the outer retina is further substantiated by an increase of lipids which engages both the outer retina and inner choroid as described in the course of AMD (Álvarez-Barrios et al. 2025). This is likely to be a consequence of the loss in Beclin1 which plays a critical role in removing lipid aggregates (Guo et al. 2026). These effects are achieved through the combined action of Beclin1 and LC3 (Guo et al. 2026).

The role of the protein Beclin1 in the retina is increasingly recognized to be pivotal for sustaining retinal integrity. In fact, Beclin1 apart from acting as a general autophagy inducer appears to sort profound effects on lipophagy, autophagy and mitophagy. In detail, the removal of Beclin1 from the Beclin1/Bcl-2 complex leads to the formation of a multi-protein complex (known as Beclin1VPS34-VPS15), which stimulates autophagy. Beclin1 plays a pivotal role in lipid metabolism, and, via VPS proteins, in binding lipid droplets to autophagosomes. In fact, the interaction of Beclin1 with VPS is crucial in inducing lipophagy. Consistently, the effects of ceramide as a powerful and specific lipophagy activator are based on Beclin1. In fact, ceramide promotes the removal of Beclin1 from the Beclin1/Bcl-2 complex, and promotes the interaction of Beclin1/VPS34/VPS15 forming a complex which is a strong lipophagy stimulator (Li et al. 2014). The activity of Beclin1 in AMD is crucial since it leads to autophagy stimulation and counteracts disease progression. Recently the expression of Beclin1 was shown to be induced by red light exposure (Stefenon et al. 2021). In detail, amber/red/infra-red light exposure owing a wavelength between 590 nm and 630 nm stimulates the expression of Beclin1 (Choi et al. 2016). This justifies the use of photobiomodulation to sustain retinal integrity. Similarly, blue led light (460 nm) when applied for short time-intervals produces a two-fold increase of the protein Beclin1 within rat retina (Wei et al. 2018). Such an increase is neuroprotective and it is well evident following

immunohistochemistry within RPE which is consistent with the present investigation linking RPE degeneration to deficient Beclin1 expression. Remarkably, blue light increases Beclin1 also in RGC (Xia et al. 2019). It is remarkable that such an increase in Beclin1 confers protection against blue light induced retinal degeneration, which markedly suppress integrity of ONL and INL, when applied for long time intervals (Wei et al. 2018; Suárez-Barrio et al. 2021). Strikingly, blue light-induced damage is markedly worsened in young (six weeks) Beclin1 deficient mice (Chen et al. 2013).

It was hypothesized that Beclin1 exerts a critical effect by acting in the context of non-canonical autophagy where, under Beclin1 stimulation the POS is phagocytosed by RPE through LAP (Ferguson and Green 2014). This may suggest a causal link between the loss of RPE65 in Beclin-1 deficient mice described in the present study. In fact, Liu et al. (2025a, b) demonstrated that LC3-associated phagocytosis (LAP) is crucial for the visual cycle recruiting the cross talk between POS and RPE which is altered in AMD. The relevant effects played by Beclin1 in sustaining retinal integrity are likely to be constantly active which is explained by the constant formation of oxidative species (Mohlin et al. 2014).

Remarkably, here we describe a pathological condition which mimics AMD though extending beyond the choroid/retinal border to recruit downstream retinal layers placed in the inner retina. This suggests that retinal degeneration is progressing downstream according to those final common pathways which involve maladaptive plasticity occurring within ONL, INL and eventually the GCL. In line with this, in these aged BECN+/- mice the most severe neuronal loss is counted within ONL and to a less extent within INL as reported for late stages of most retinal degenerative disorders. This confirms findings in humans affected by AMD, where early pathology appears to be confined to the outer retina, while disease progression leads to the involvement of inner retina with a thinning of both ONL and INL (Farinha et al. 2021).

The involvement of the inner retina in aged BECN+/- mice is not unexpected considering that most retinal degenerative disorders start in the outer retina and may extend along the macular and extra-macular regions along external retinal surface to progress from the outer to the inner retina according to a trans-synaptic transmission which starts from outer retinal layer to recruit a sort of maladaptive plasticity within inner retinal layers. For instance, in the case of the most common degeneration, AMD typically affects the macular region of the retina and it is clinically characterized by a progressive loss of visual acuity, impaired color perception, and diminished contrast sensitivity. A hallmark symptom is blurred central vision which is accompanied by metamorphopsia, where horizontal or vertical lines appear distorted (Christoforidis et al. 2011; Randolph 2024; Roh et al. 2018). The pathology of AMD starts from the outer retina, specifically at the border between outer retina and inner choroid. This area is known as retinal neurovascular unit (RNVU) (Pinelli et al. 2023; Grimes et al. 2025) and it is composed of the outer segment of photoreceptors (POS), the retinal pigment epithelium (RPE), and the choriocapillaris (CC). Among these layers, the retinal pigment epithelium (RPE) is mostly affected at early stages of retinal degeneration (Pfeiffer et al. 2020a, b, c). According to these studies, late degeneration of AMD spreads from external to internal layers progressing downstream through retinal neuronal chains. This progression reminds typical central degenerative disorders to produce non-specific trans-synaptic retinal degeneration, which becomes quite independent from the primary site involved in the degenerative disease (Pfeiffer et al. 2020a, b, c). This latter phenomenon represents a sort of maladaptive plasticity which carries cell pathology from the outer to the inner retina (Marc et al. 2003; Pfeiffer et al. 2020a, b, c). Maladaptive plasticity should be considered as a kind of retina remodeling, where compensatory changes indeed bring a detrimental plasticity. This happens also during retinitis pigmentosa. At late stages, these disorders produce a downstream pathological remodeling which becomes quite independent from the early pathological events and may even overlap with classic degenerative conditions affecting the CNS (Pfeiffer et al. 2020a, b, c; Pinelli et al. 2025). The kind of central neurodegenerative disorders which are mimicked at late stages of retinal degeneration are reminiscent of the so-called proteinopathies. This is because the specific degeneration of the outer retina converges into the loss of photoreceptor to involve the inner segment along the nucleus in the axon, which is recapitulated by the present findings showing a severe loss of cell and nuclear density within ONL. The synapse with bipolar cells is a critical site to transmit pathology which here is evident by a significant cell loss of bipolar cells as evidence by a loss of INL cells and nuclei. It is likely that a loss of photoreceptors may drive trans-synaptic alterations sustained by deafferentation of bipolar cells. This phenomenon may often be described in humans since it develops over time. The present study was the first to assess the long-term effects generated in aged mice. Remarkably, a protein constituent which is sensing downstream progression is alpha-syn, which extends to the inner retina during AMD as a classic synucleinopathy. Thus, a defect of Beclin1 is likely to pave the way to a detrimental metabolism in the outer retina which is no longer capable of degrading and recycling damaged cellular components. It is likely that Beclin1 play a significant role in AMD pathogenesis, particularly due to its impaired activity in the disease state (Jun et al. 2019; Kaarniranta et al. 2023).

The progression of the disease may shift towards a trans-synaptic proteinopathy.

In fact, alpha-synuclein aggregates do not occur in the outer retina at early stages of AMD, although at later stages the detrimental protein alpha-syn, increases downstream in the inner retina (Pfeiffer et al. 2020a, b, c; Pinelli et al. 2025) suggesting a protein spreading which induces a shift in the maturation of the disease. Not surprisingly, in the present study the protein alpha-syn increases dramatically in the inner retina staring from the ONL. The occurrence of late stage proteinopathy and the disease mechanisms early affecting the outer retina suggest that a defect in Beclin1 plays a pivotal role both in altering autophagy and possibly affecting non-autophagy dependent pathways. This is in line with the concept that Beclin 1 plays a critical role in removing lipids and recycling mitochondria through an interaction with AMBRA1 (Ramírez-Pardo et al. 2023; Di Rienzo et al. 2024; Hansman et al. 2025). The effective role of Beclin1 in safeguarding the outer retina especially within RPE cells may extend to pathways alternative to Pink1-Parkin interaction, (Hyttinen et al. 2021; D'Amico et al. 2024; Pinelli et al. 2025). Despite the promising role of Beclin1 in sustaining retinal integrity and counteracting AMD, the present study represents the first documentation of whether a genetic depletion of Beclin1 when assessed in aged mammals may mimic AMD. The subcellular analysis and fine ultrastructure will help to clarify the specific cell compartments being affected by the loss of Beclin1. For instance, due to a role of Beclin1 at the intersection between mitochondrial removal, lipid metabolism, and sugar turnover it would be worthy to investigate at electron microscopy the amount of lipid droplets, glycogen granules and the kind of mitochondrial alterations, which are produced in the deficiency of Beclin1. All these structures are strongly altered in the course of AMD. Just like AMD, retinal pathology in Beclin1 deficient mice does not feature alpha-syn increase within outer retinal neurons, while the inner retina at later stages develop a synucleinopathy. This hypothesis may represent the starting point to develop novel therapeutic strategies to modify retinal disease progression and quenching the natural course of central degenerative disorders. In line with this, a reduced expression of Beclin1 is correlated with age-related autophagosome formation in the aged mouse retina. This is supposed to produce age-dependent depotentiation of canonical autophagy which adds on the loss of effects fostered by Beclin1 in non-canonical autophagy pathways (Lenzi et al. 2003). This is confirmed by the absence of retinal pathology neither in the RPE nor in the inner retina, including ONL and INL, in BECN+/- at the age of 6 weeks (Chen et al. 2013) and 2 months (Chen et al. 2013), which was confirmed here in pilot staining. The chance to elevate Beclin1 in the aged retina may represent a tool to counteract retinal degeneration. This may be achieved through exposure to long wavelengths, such as pure red light. This amber/red light exerts a powerful antioxidant effect, per se, and through the activation of the inducible isoform of the chaperone protein heat shock protein 70 (HSP70). In addition, red light activates autophagy and removes specific autophagy substrates such as the misfolded proteins (Comerota et al. 2019; Yang et al. 2021). This is confirmed by the fact, that Beclin1 suddenly increases following red light exposure. Such an approach may be used through photobiomodulation to prevent or counteract age-dependent retinal degeneration.

Supplementary Information The online version contains supplementary material available at https://doi.org/10.1007/s00702-026-03166-4.

Author contributions Breeding, maintenance and care of mice used for experimental procedures, M.F. and F.D.; Generation of light microscopy data, F.B. and C.L.B.; RT-PCR and western blot, M.F. and F.D.; Data analysis, F.B., C.L.B., M.F., F.D. Statistics: G.L., M.F.; Writing manuscript draft: F.B, C.L.B., F.F.; Conceptualization: R.P., V.V.B., S.S., G.F., F.F.; Supervision and funding acquisition: F.F.; Artwork: F.B., C.L.B., M.F.; Revising manuscript draft: F.B., C.L.B., F.F.; Editing final manuscript: F.B., C.L.B. All authors have read and agreed to the published version of the manuscript.

Funding Ricerca Corrente 2026, Ministero della Salute, IRCCS Neuromed.

Data availability The rough data of this study are uploaded in a repository which will be made available at a website to be created by the corresponding author upon request.

Declarations

Conflict of interest The authors declare no competing interests. The authors have no relevant financial or non-financial interests to disclose.

References

Álvarez-Barrios A, Álvarez L, de Sáenz P, García M, Álvarez-Buylla JR, Pereiro R, González-Iglesias H (2025) Dysregulated lipid metabolism in a retinal pigment epithelial cell model and serum of patients with age-related macular degeneration. BMC Biol 23:96. https://doi.org/10.1186/s12915-025-02198-8

Augustin AJ, Kirchhof J (2009) Inflammation and the pathogenesis of age-related macular degeneration. Expert Opin Ther Targets 13:641–651. https://doi.org/10.1517/14728220902942322

Bammidi S, Ghosh S, Chowdhury O, Babu VS, Dutta P, Hose S, Sinha D (2025) MLST8 overexpression in RPE cells disrupts autophagy through novel mechanisms affecting AMD pathogenesis. Autophagy 21:1856–1858. https://doi.org/10.1080/15548627.2025.2491097

Battaglia G, Busceti CL, Pontarelli F, Biagioni F, Fornai F, Paparelli A, Bruno V, Ruggieri S, Nicoletti F (2003) Protective role of group-II metabotropic glutamate receptors against nigro-striatal degeneration induced by 1-methyl-4-phenyl-1,2,3,6-tetrahydropyridine

in mice. Neuropharmacology 45:155–166. https://doi.org/10.1016/s0028-3908(03)00146-1
Blasiak J, Kaarniranta K (2022) Secretory autophagy: a turn key for understanding AMD pathology and developing new therapeutic targets? Expert Opin Ther Targets 26:883–895. https://doi.org/10.1080/14728222.2022.2157260
Bruban J, Glotin AL, Dinet V, Chalour N, Sennlaub F, Jonet L, An N, Faussat AM, Mascarelli F (2009) Amyloid-beta(1–42) alters structure and function of retinal pigmented epithelial cells. Aging Cell 8:162–177. https://doi.org/10.1111/j.1474-9726.2009.00456.x
Chen Y, Sawada O, Kohno H, Le YZ, Subauste C, Maeda T, Maeda A (2013) Autophagy protects the retina from light-induced degeneration. J Biol Chem 288:7506–7518. https://doi.org/10.1074/jbc.M112.439935
Choi MS, Kim HJ, Ham M, Choi DH, Lee TR, Shin DW (2016) Amber Light (590 nm) induces the breakdown of lipid droplets through autophagy-related lysosomal degradation in differentiated adipocytes. Sci Rep 6:28476. https://doi.org/10.1038/srep28476
Chowdhury O, Bammidi S, Gautam P, Babu VS, Liu H, Shang P, Xin Y, Mahally E, Nemani M, Koontz V et al (2025) Activated mTOR signaling in the RPE drives EMT, autophagy, and metabolic disruption, resulting in AMD-like pathology in mice. Aging Cell 17:e70018. https://doi.org/10.1111/acel.70018
Christoforidis JB, Tecce N, Dell'Omo R, Mastropasqua R, Verolino M, Costagliola C (2011) Age related macular degeneration and visual disability. Curr Drug Targets 12:221–233. https://doi.org/10.2174/138945011794182755
Comerota MM, Tumurbaatar B, Krishnan B, Kayed R, Taglialatela G (2019) Near infrared light treatment reduces synaptic levels of toxic tau oligomers in two transgenic mouse models of human tauopathies. Mol Neurobiol 56:3341–3355. https://doi.org/10.1007/s12035-018-1248-9
D'Amico AG, Maugeri G, Magrì B, Bucolo C, D'Agata V (2024) Targeting the PINK1/Parkin pathway: a new perspective in the prevention and therapy of diabetic retinopathy. Exp Eye Res 247:110024. https://doi.org/10.1016/j.exer.2024.110024
Datta S, Cano M, Satyanarayana G, Liu T, Wang L, Wang J, Cheng J, Itoh K, Sharma A, Bhutto I, Kannan R, Qian J, Sinha D, Handa JT (2023) Mitophagy initiates retrograde mitochondrial-nuclear signaling to guide retinal pigment cell heterogeneity. Autophagy 19:966–983. https://doi.org/10.1080/15548627.2022.2109286
Di Rienzo M, Romagnoli A, Refolo G, Vescovo T, Ciccosanti F, Zuchegna C, Lozzi F, Occhigrossi L, Piacentini M, Fimia GM (2024) Role of AMBRA1 in mitophagy regulation: emerging evidence in aging-related diseases. Autophagy 20:2602–2615. https://doi.org/10.1080/15548627.2024.2389474
Du Y, Xia Y (2025) Retinal pigment epithelium phagocytosis and retinal degenerative diseases. Aging Dis https://doi.org/10.14336/AD.2025.0542
Duncan JL, Bowman A, Laster A, Gelfman C, Birch DG, Boye SE, Daiger SP, Del Priore L, Zack DJ, Handa JT (2024) Foundation fighting blindness scientific advisory board. inherited retinal degenerations and non-neovascular age-related macular degeneration: progress and unmet needs. Transl Vis Sci Technol 13:28. https://doi.org/10.1167/tvst.13.12.28
Etchegaray JI, Ravichandran K (2025) Role of RPE phagocytosis in the retina metabolic ecosystem. Adv Exp Med Biol 1468:429–433. https://doi.org/10.1007/978-3-031-76550-6_70
Fang J, Huang Y, Li B, Du Y (2026) Role and regulation of kinases in age-related macular degeneration. J Transl Med 24:227. https://doi.org/10.1186/s12967-025-07669-8
Farinha C, Silva AL, Coimbra R, Nunes S, Cachulo ML, Marques JP, Pires I, Cunha-Vaz J, Silva R (2021) Retinal layer thicknesses and neurodegeneration in early age-related macular degeneration: insights from the Coimbra Eye Study. Graefes Arch Clin Exp Ophthalmol 259:2545–2557. https://doi.org/10.1007/s00417-021-05140-0
Ferguson TA, Green DR (2014) Autophagy and phagocytosis converge for better vision. Autophagy 10:165–167. https://doi.org/10.4161/auto.26735
Furuse M, Hirase T, Itoh M, Nagafuchi A, Yonemura S, Tsukita S, Tsukita S (1993) Occludin: a novel integral membrane protein localizing at tight junctions. J Cell Biol 123:1777–1788. https://doi.org/10.1083/jcb.123.6.1777
Georgiadis A, Tschernutter M, Bainbridge JW, Balaggan KS, Mowat F, West EL, Munro PM, Thrasher AJ, Matter K, Balda MS, Ali RR (2010) The tight junction associated signalling proteins ZO-1 and ZONAB regulate retinal pigment epithelium homeostasis in mice. PLoS ONE 5:e15730. https://doi.org/10.1371/journal.pone.0015730
Ghasemi M, Ghasemi A, Behjati J, Nikkhah H (2026) Association between diabetic retinopathy and age-related macular degeneration: a systematic review and meta-analysis. Graefes Arch Clin Exp Ophthalmolhttps://doi.org/10.1007/s00417-026-07119-1
Golestaneh N, ChuY, Xiao YY, Stoleru GL, Theos AC (2017) Dysfunctional autophagy in RPE, a contributing factor in age-related macular degeneration. Cell Death Dis 8:e2537. https://doi.org/10.1038/cddis.2016.453
Grimes WN, Berson DM, Sabnis A, Hoon M, Sinha R, Tian H, Diamond JS (2025) Layer-specific anatomical and physiological features of the retina's neurovascular unit. Curr Biol 35:109–120e4. https://doi.org/10.1016/j.cub.2024.11.023
Guo X, Yin X, Liu Z, Wang J (2026) Hepatoprotective effects of tetrahydropalmatine against NAFLD through autophagy activation and lipid metabolic reprogramming via the AMPK-mTOR-Sirt1 axis. J Ethnopharmacol 360:121217. https://doi.org/10.1016/j.jep.2026.121217
Gurubaran IS, Watala C, Kostanek J, Szczepanska J, Pawlowska E, Kaarniranta K, Blasiak J (2024) PGC-1α regulates the interplay between oxidative stress, senescence and autophagy in the ageing retina important in age-related macular degeneration. J Cell Mol Med 28:e18051. https://doi.org/10.1111/jcmm.18051
Hansman DS, Du J, Casson RJ, Peet DJ (2025) Eye on the horizon: the metabolic landscape of the RPE in aging and disease. Prog Retin Eye Res 104:101306. https://doi.org/10.1016/j.preteyeres.2024.101306
Hartsock A, Nelson WJ (2008) Adherens and tight junctions: structure, function and connections to the actin cytoskeleton. Biochim Biophys Acta 1778:660–669. https://doi.org/10.1016/j.bbamem.2007.07.012
Hyttinen J, Blasiak J, Tavi P, Kaarniranta K (2021) Therapeutic potential of PGC-1α in age-related macular degeneration (AMD) - the involvement of mitochondrial quality control, autophagy, and antioxidant response. Expert Opin Ther Targets 25:773–785. https://doi.org/10.1080/14728222.2021.1991913
Jarocki M, Turek K, Saczko J, Tarek M, Kulbacka J (2024) Lipids associated with autophagy: mechanisms and therapeutic targets. Cell Death Discov 10:460. https://doi.org/10.1038/s41420-024-02224-8
Jiang F, Ma J, Lei C, Zhang Y, Zhang M (2025) Age-related macular degeneration: cellular and molecular signaling mechanisms. Int J Mol Sci 26:6174. https://doi.org/10.3390/ijms26136174
Jun S, Datta S, Wang L, Pegany R, Cano M, Handa JT (2019) The impact of lipids, lipid oxidation, and inflammation on AMD, and the potential role of miRNAs on lipid metabolism in the RPE. Exp Eye Res 181:346–355. https://doi.org/10.1016/j.exer.2018.09.023
Kaarniranta K, Blasiak J, Liton P, Boulton M, Klionsky DJ, Sinha D (2023) Autophagy in age-related macular degeneration. Autophagy 19:388–400. https://doi.org/10.1080/15548627.2022.2069437

Kim J, Moon SY, Kang HG, Kim HJ, Choi JS, Lee SHS, Park K, Won SY (2025) Therapeutic potential of AAV2-shmTOR gene therapy in reducing retinal inflammation and preserving endothelial Integrity in age-related macular degeneration. Sci Rep 15:9517. https://doi.org/10.1038/s41598-025-93993-4

Koutsifeli P, Varma U, Daniels LJ, Annandale M, Li X, Neale JPH, Hayes S, Weeks KL, James S, Delbridge LMD et al (2022) Glycogen-autophagy: molecular machinery and cellular mechanisms of glycophagy. J Biol Chem 298:102093. https://doi.org/10.1016/j.jbc.2022.102093

Kubicka-Trzaska A, Zuber-Laskawiec K, Plutecka H, Romanowska-Dixon B, Sanak M, Karska-Basta I (2021) Altered serum levels of autophagy proteins Beclin-1 and mTOR in patients with exudative age-related macular degeneration. J Physiol Pharmacol https://doi.org/10.26402/jpp.2021.1.09. Epub 2021 Feb 21. PMID: 34099588

Lazzeri G, Lenzi P, Busceti CL, Ferrucci M, Falleni A, Bruno V, Paparelli A, Fornai F (2007) Mechanisms involved in the formation of dopamine-induced intracellular bodies within striatal neurons. J Neurochem 101:1414–1427. https://doi.org/10.1111/j.1471-4159.2006.04429.x

Lazzeri G, Ferrucci M, Lenzi P, Giambelluca MA, Biagioni F, Busceti CL, Frati A, Fornai F (2025) Modulation of mtor within retinal pigment epithelium affects cell viability and mitochondrial pathology. Int J Mol Sci 26:9442. https://doi.org/10.3390/ijms26199442

Lenzi P, Frenzilli G, Gesi M, Ferrucci M, Lazzeri G, Fornai F, Nigro M (2003) DNA damage associated with ultrastructural alterations in rat myocardium after loud noise exposure. Environ Health Perspect 111:467–471. https://doi.org/10.1289/ehp.5847

Lenzi P, Lazzeri G, Biagioni F, Busceti CL, Gambardella S, Salvetti A, Fornai F (2016) The autophagoproteasome a Novel cell clearing organelle in baseline and stimulated conditions. Front Neuroanat 10:78. https://doi.org/10.3389/fnana.2016.00078

Li Y, Li S, Qin X, Hou W, Dong H, Yao L, Xiong L (2014) The pleiotropic roles of sphingolipid signaling in autophagy. Cell Death Dis https://doi.org/10.1038/cddis.2014.215. Erratum in: Cell Death Dis 5:e1415

Li H, Sharma R, Bharti K (2025) iPSC-derived retinal pigment epithelium: an in vitro platform to reproduce key cellular phenotypes and pathophysiology of retinal degenerative diseases. Stem Cells Transl Med 14:szae097. https://doi.org/10.1093/stcltm/szae097

Libby RT, Gould DB (2010) Endoplasmic reticulum stress as a primary pathogenic mechanism leading to age-related macular degeneration. Adv Exp Med Biol 664:403–409. https://doi.org/10.1007/978-1-4419-1399-9_46

Limanaqi F, Biagioni F, Gaglione A, Busceti CL, Fornai F (2019) A sentinel in the crosstalk between the nervous and immune system: the (Immuno)-proteasome. Front Immunol 10:628. https://doi.org/10.3389/fimmu.2019.00628

Liu D, Zhang C, Zhang J, Xu GT, Zhang J (2023) Molecular pathogenesis of subretinal fibrosis in neovascular AMD focusing on epithelial-mesenchymal transformation of retinal pigment epithelium. Neurobiol Dis 185:106250. https://doi.org/10.1016/j.nbd.2023.106250

Liu M, Wang Y, Ren F, Zhang W, Zheng H, Zhang R, Gao C, Luo L, Nie C, Gu J (2025a) Simulated microgravity activates autophagy expression in the rat retina. Life Sci Space Res (Amst) 45:107–116. https://doi.org/10.1016/j.lssr.2025.02.004

Liu F, Li Q, Yang Y, Lu F (2025b) Visual cycle and LC3-associated phagocytosis in retina: regulatory mechanisms and therapeutic potential. Biomed Pharmacother 190:118423. https://doi.org/10.1016/j.biopha.2025.118423

Ma JYW, Greferath U, Wong JHC, Fothergill LJ, Jobling AI, Vessey KA, Fletcher EL (2023) Aging induces cell loss and a decline in phagosome processing in the mouse retinal pigment epithelium. Neurobiol Aging 128:1–16. https://doi.org/10.1016/j.neurobiolaging.2023.03.003

Mancini MC, Noland RC, Collier JJ, Burke SJ, Stadler K, Heden TD (2023) Lysosomalglucose sensing and glycophagy in metabolism. Trends Endocrinol Metab 34:764–777

Marc RE, Jones BW, Watt CB, Strettoi E (2003) Neural remodeling in retinal degeneration. Prog Retin Eye Res. https://doi.org/10.1016/s1350-9462(03)00039-9. 22:607–55

Markitantova Y, Simirskii V (2025) Retinal pigment epithelium under oxidative stress: chaperoning autophagy and beyond. Int J Mol Sci 26:1193. https://doi.org/10.3390/ijms26031193

Modenese A, Gobba F (2019) Macular degeneration and occupational risk factors: a systematic review. Int Arch Occup Environ Health 92:1–11. https://doi.org/10.1007/s00420-018-1355-y

Mohlin C, Taylor L, Ghosh F, Johansson K (2014) Autophagy and ER-stress contribute to photoreceptor degeneration in cultured adult porcine retina. Brain Res. https://doi.org/10.1016/j.brainres.2014.08.055. 1585:167–83

Mohtashami Z, Schneider K, Azimi R, Atilano S, Chwa M, Kenney MC, Singh MK (2025) Exploring the therapeutic potential of MOTS-c in age-related macular degeneration: from cellular responses to patient-derived cybrids. Hum Cell 38:57. https://doi.org/10.1007/s13577-025-01188-w

Molins B, Pascual A, Méndez AP, Llorenç V, Zarranz-Ventura J, Mesquida M, Adán A, Martorell J (2017) C-reactive protein isoforms differentially affect outer blood-retinal barrier integrity and function. Am J Physiol Cell Physiol 312:C244–C253. https://doi.org/10.1152/ajpcell.00057.2016

Napoli D, Strettoi E (2023) Structural abnormalities of retinal pigment epithelial cells in a light-inducible, rhodopsin mutant mouse. J Anat 243:223–234. https://doi.org/10.1111/joa.13667

Napoli D, Biagioni M, Billeri F, Di Marco B, Orsini N, Novelli E, Strettoi E (2021) Retinal Pigment Epithelium Remodeling in Mouse Models of Retinitis Pigmentosa. Int J Mol Sci. 2021 22:5381. https://doi.org/10.3390/ijms22105381

Nita M, Grzybowski A (2023) Antioxidative role of heterophagy, autophagy, and mitophagy in the retina and their association with the Age-Related Macular Degeneration (AMD) etiopathogenesis. Antioxidants (Basel). 12:1368. https://doi.org/10.3390/antiox12071368

Pan HY, Valapala M (2023) Role of TFEB in diseases associated with lysosomal dysfunction. Adv Exp Med Biol 1415:319–325. https://doi.org/10.1007/978-3-031-27681-1_46

Pfeiffer RL, Marc RE, Jones BW (2020a) Persistent remodeling and neurodegeneration in late-stage retinal degeneration. Prog Retin Eye Res 74:100771. https://doi.org/10.1016/j.preteyeres.2019.07.004

Pfeiffer RL, Marc RE, Jones BW (2020b) Müller cell metabolic signatures: evolutionary conservation and disruption in disease. Trends Endocrinol Metab 31:320–329. https://doi.org/10.1016/j.tem.2020.01.005

Pfeiffer RL, Anderson JR, Dahal J, Garcia JC, Yang JH, Sigulinsky CL, Rapp K, Emrich DP, Watt CB, Johnstun HA, Houser AR, Marc RE, Jones BW (2020c) A pathoconnectome of early neurodegeneration: network changes in retinal degeneration. Exp Eye Res 199:108196. https://doi.org/10.1016/j.exer.2020.108196

Pinelli R, Ferrucci M, Berti C, Biagioni F, Scaffidi E, Bumah VV, Busceti CL, Lenzi P, Lazzeri G, Fornai F (2023) The essential role of light-induced autophagy in the inner choroid/outer retinal neurovascular unit in baseline conditions and degeneration. Int J Mol Sci 24:8979. https://doi.org/10.3390/ijms24108979

Pinelli R, Lazzeri G, Berti C, Biagioni F, Scaffidi E, Ferrucci M, Bumah VV, Fornai F (2025) Retinal autophagy for sustaining retinal integrity as a proof of concept for age-related macular degeneration. Int J Mol Sci 26:5773. https://doi.org/10.3390/ijms26125773

Postnikova OA, William S, Uppal S, Bernstein SL, Poliakov E, Rogozin IB, Edmond TM (2025) Regulation of RPE65 expression in human retinal pigment epithelium cells. Sci Rep 15:27106. https://doi.org/10.1038/s41598-025-12926-3

Ramírez-Pardo I, Villarejo-Zori B, Jiménez-Loygorri JI, Sierra-Filardi E, Alonso-Gil S, Mariño G, de la Villa P, Fitze PS, Fuentes JM, García-Escudero R, Ferrington DA, Gomez-Sintes R, Boya P (2023) Ambra1 haploinsufficiency in CD1 mice results in metabolic alterations and exacerbates age-associated retinal degeneration. Autophagy 19:784–804. https://doi.org/10.1080/15548627.2022.2103307

Randolph SA (2024) Age-related macular degeneration. Workplace Health Saf 62:352. https://doi.org/10.1177/21650799140620080 7

Roh M, Selivanova A, Shin HJ, Miller JW, Jackson ML (2018) Visual acuity and contrast sensitivity are two important factors affecting vision-related quality of life in advanced age-related macular degeneration. PLoS ONE 13:e0196481. https://doi.org/10.1371/journal.pone.0196481

Ryskalin L, Gaglione A, Limanaqi F, Biagioni F, Familiari P, Frati A, Esposito V, Fornai F (2019) The autophagy status of cancer stem cells in gliobastoma multiforme: from cancer promotion to therapeutic strategies. Int J Mol Sci 20:3824. https://doi.org/10.3390/ijms20153824

Shatz N, Chohan Y, Klionsky DJ (2024) ATG14 and STX18: gatekeepers of lipid droplet degradation and the implications for disease modulation. Autophagy 20:1697–1699. https://doi.org/10.1080/15548627.2024.2350739

Singh R, Cuervo AM (2012) Lipophagy: connecting autophagy and lipid metabolism. Int J Cell Biol 2012:282041. https://doi.org/10.1155/2012/282041

Squitieri F, Falleni A, Cannella M, Orobello S, Fulceri F, Lenzi P, Fornai F (2010) Abnormal morphology of peripheral cell tissues from patients with Huntington disease. J Neural Transm (Vienna) 117:77–83. https://doi.org/10.1007/s00702-009-0328-4

Stefenon L, Boasquevisque M, Garcez AS, de Araújo VC, Soares AB, Santos-Silva AR, Sperandio F, Brod JMM, Sperandio M (2021) Autophagy upregulation may explain inhibition of oral carcinoma in situ by photobiomodulation in vitro. J Photochem Photobiol 221:112245. https://doi.org/10.1016/j.jphotobiol.2021.112245

Suárez-Barrio C, Del Olmo-Aguado S, García-Pérez E, Fernández-Vega-Cueto L, Fernández-Vega Cueto A, Baamonde-Arbaiza B, Fernández-Vega L, Merayo-Lloves J (2021) Plasma rich in growth factors promotes autophagy in ARPE19 cells in response to oxidative stress induced by blue light. Biomolecules 11:954. https://doi.org/10.3390/biom11070954

Sze YH, Zuo B, Lu DQ, Li KK, Tse DYY, Zhao Q, Lam TC (2025) Comparative analysis of ocular biometrics using spectral domain optical coherence tomography with Purkinje image and optic nerve head alignments in mice. Eur J Med Res 30:67. https://doi.org/10.1186/s40001-025-02305-z

Tanabu R, Sato K, Monai N, Yamauchi K, Gonome T, Xie Y, Takahashi S, Ishiguro SI, Nakazawa M (2019) The findings of optical coherence tomography of retinal degeneration in relation to the morphological and electroretinographic features in RPE65-/- mice. PLoS ONE 14:e0210439. https://doi.org/10.1371/journal.pone.0210439

Wang S, Wang X, Cheng Y, Ouyang W, Sang X, Liu J, Su Y, Liu Y, Li C, Yang L, Jin L, Wang Z (2019) Autophagy dysfunction, cellular senescence, and abnormal immune-inflammatory responses in AMD: from mechanisms to therapeutic potential. Oxid Med Cell Longev https://doi.org/10.1155/2019/3632169

Wang L, Wang LX, Li MY, Zhang R, Zhou GH (2025) Clinical characterization of CCT2 and its role in autophagy regulation during age-related macular degeneration. Sci Rep 15:16849. https://doi.org/10.1038/s41598-025-01907-1

Wei Q, Liang X, Peng Y, Yu D, Zhang R, Jin H, Fan J, Cai W, Ren C, Yu J (2018) 17β-estradiol ameliorates oxidative stress and blue light-emitting diode-induced retinal degeneration by decreasing apoptosis and enhancing autophagy. Drug Des Devel Ther 12:2715–2730. https://doi.org/10.2147/DDDT.S176349

Wert KJ, Lin JH, Tsang SH (2014) General pathophysiology in retinal degeneration. Dev Ophthalmol 53:33–43. https://doi.org/10.1159/000357294

Wolfensberger TJ, Gregor ZJ (2010) Macular edema-rationale for therapy. Dev Ophthalmol 47:49–58. https://doi.org/10.1159/000320073

Xia H, Hu Q, Li L, Tang X, Zou J, Huang L, Li X (2019) Protective effects of autophagy against blue light-induced retinal degeneration in aged mice. Sci China Life Sci 62:244–256. https://doi.org/10.1007/s11427-018-9357-y

Yang KL, Khoo BY, Ong MT, Yoong ICK, Sreeramanan S (2021) In vitro anti-breast cancer studies of LED red light therapy through autophagy. Breast Cancer 28:60–66. https://doi.org/10.1007/s12282-020-01128-6

Yang X, Xu W, Xie H, Guo X, Zhu F, Xing Y, Chen C (2026) The contribution of ferroptosis to the epithelial-mesenchymal transition phenotype in models of age-related macular degeneration. Front Cell Dev Biol 14:1718715. https://doi.org/10.3389/fcell.2026.1718715

Yao J, Jia L, Khan N, Lin C, Mitter SK, Boulton ME, Dunaief JL, Klionsky DJ, Guan JL, Thompson DA, Zacks DN (2015) Deletion of autophagy inducer RB1CC1 results in degeneration of the retinal pigment epithelium. Autophagy 11:939–953. https://doi.org/10.1080/15548627.2015.1041699

Zhang H, Fan J, Li S, Karan S, Rohrer B, Palczewski K, Frederick JM, Crouch RK, Baehr W (2018) Trafficking of membrane-associated proteins to cone photoreceptor outer segments requires the chromophore 11-cis-retinal. J Neurosci 28:4008–4014. https://doi.org/10.1523/JNEUROSCI.0317-08.2008

Zhang SM, Fan B, Li YL, Zuo ZY, Li GY (2023) Oxidative stress-involved mitophagy of retinal pigment epithelium and retinal degenerative diseases. Cell Mol Neurobiol 43:3265–3276. https://doi.org/10.1007/s10571-023-01383-z

Zhang Z, Shan X, Liang F, Fang L (2026) Integrative single-cell transcriptomic and experimental analyses unveil Qihuang granule's protection against retinal photodamage via PI3K/AKT/mTOR-mediated autophagy. Int J Biochem Cell Biol 190:106881. https://doi.org/10.1016/j.biocel.2025.106881

Zhou S, Taskintuna K, Hum J, Gulati J, Olaya S, Steinman J, Golestaneh N (2024) PGC-1α repression dysregulates lipid metabolism and induces lipid droplet accumulation in retinal pigment epithelium. Cell Death Dis 15:385. https://doi.org/10.1038/s41419-024-06762-y

Zihni C (2025) Phagocytosis by the retinal pigment epithelium: new insights into polarized cell mechanics. BioEssays 47:e2300197. https://doi.org/10.1002/bies.202300197